國立臺灣大學生物資源暨農學院農業化學系

碩士論文

Department of Agricultural Chemistry

College of Bioresources and Agriculture

National Taiwan University

Master Thesis

銅鐵雙金屬奈米顆粒結合 Fenton 反應接續礦化移除

四溴雙酚 A

Removal of tetrabromobisphenol A by Cu/Fe bimetallic

nanoparticles and sequential mineralization with a

Fenton reaction

郭進順

Chin-shun Kuo

指導教授：施養信 博士

Advisor: Yang-hsin Shih, Ph.D.

中華民國 106 年 2 月

February 2017

摘要

　　四溴雙酚 A (Tetrabromobisphenol, TBBPA)是最被廣泛使用的溴化阻燃劑，由於不當的貯存和處置，導致 TBBPA 已經在多種環境基質，甚至是人體中被偵測到。此外，許多前人研究顯示，TBBPA 可能會對人體造成負面的影響，因此，開發出一個有效的 TBBPA 整治方法是非常重要的。奈米零價鐵已經成功地被應用於處理含鹵有機汙染物，而藉著第二種金屬當催化劑，形成的雙金屬顆粒能更有效地處理含鹵有機汙染物。然而 TBBPA 降解的副產物具有類似內分泌干擾素的能力，在此研究中，也將進一步探討 Fenton 反應對於 TBBPA 脫溴副產物移除之效率。銅鐵雙金屬奈米顆粒能快速及有效地使 TBBPA 脫溴。在銅添加量上，4.0 % 的銅在銅鐵奈米顆粒上，具有最高的移除效率 99.8 %，其擬一階速率常數為 0.229 min^{-1}。此外，當銅鐵雙金屬奈米顆粒劑量增加及 TBBPA 初始濃度下降時，TBBPA 反應動力隨之上升。在 TBBPA 初始濃度為 5.0 mg/L，銅鐵雙金屬奈米顆粒劑量為 2.0 g/L 時，TBBPA 在 30 分鐘內會被完全移除，在反應期間，較低溴數的副產物和溴離子會被偵測到。銅鐵雙金屬奈米顆粒移除 TBBPA 之反應速率隨溫度增加而增加，並計算出活化能為 35.64 kJ/mole，顯示此反應為表面控制之作用。在水溶液 pH 值的影響上，銅鐵雙金屬奈米顆粒較偏好在酸性環境下移除 TBBPA。當 pH 值從 9.0 降低到 5.0 時，反應速率常數從 0.191 min^{-1} 增加到 0.228 min^{-1}，pH 值持續地下降到 3.0 時，反應速率常數則會下降至 0.162 min^{-1}。另外，在 pH 3.0 到 pH 9.0 間，其 TBBPA 的移除效率無顯著差異，皆高於 98.5 %。然而，在 pH 11.0 時，其移除效率及反應速率常數則分別只有 77.0 % 和 0.063 min^{-1}。Cu/Fe 雙金屬奈米顆粒可將 TBBPA 完全脫溴，藉由其脫溴副產物：三溴雙酚 A、二溴雙酚 A、一溴雙酚 A 及雙酚 A (BisphenolA, BPA) 推測出其降解途徑。原則上，藉由銅鐵雙金屬奈米顆粒反應後鐵氧化生成的鐵離子及額外添加的 H_2O_2，使 TBBPA 脫溴最終副產物 BPA 可利用 Fenton 反應移除。在 BPA 溶液中，增加 H_2O_2 或 Fe^{2+} 濃度，會增加 BPA 的移除速率；然而，過高的 H_2O_2 或 Fe^{2+} 濃度，會降低 BPA 的移除速率，分別為從 0.015 min^{-1} 降到 0.0107 min^{-1} 及 0.015 min^{-1} 降到 0.0004 min^{-1}。合成的銅鐵雙金屬奈米顆粒對於處理 TBBPA 有相當高的潛力，且結合 H_2O_2 能有效地礦化大部分的 TBBPA 與其脫溴副產物。

關鍵字：四溴雙酚 A、雙酚 A、銅鐵雙金屬奈米顆粒、脫溴

I

Abstract
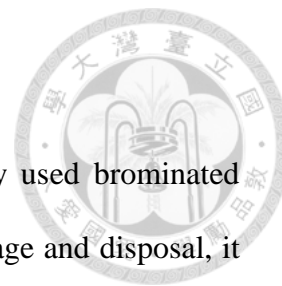
Tetrabromobisphenol A (TBBPA) is one of the most widely used brominated flame retardant. Due to its extensive usage and then improper storage and disposal, it has been detected in various environmental matrices and even human bodies. Moreover, many previous studies showed the results that TBBPA could cause many negative effects on human bodies. Thus, exploiting an effective method for TBBPA treatment is important. Nanoscale zero-valent iron has been successfully applied for treating halogenated organic pollutants. With a secondary metal as the catalyst, bimetallic nanoparticles (BNPs) become more efficient. However, the byproducts of TBBPA degradation have the ability like endocrine disruptor. In this study, we further investigated Fenton reaction for final TBBPA debrominated byproducts.

The results showed that Cu/Fe BNP aggregates demonstrated a fast and effective debromination of TBBPA. For copper doping, Cu/Fe NPs in 4.0 % copper ratio had the highest removal efficiency with a pseudo-first order rate constant of 0.229 min^{-1}. Furthermore, reaction kinetics increased as the decreased initial TBBPA concentrations and the increased dosages of Cu/Fe BNPs. At the initial TBBPA concentration of 5.0 mg L^{-1}, TBBPA could be completely removed within 30 min by a Cu/Fe NPs dosage of 2.0 g L^{-1}, and less brominated byproducts and bromide ions were detected during the reactions. The activation energy of the TBBPA removal with Cu/Fe BNPs was 35.64 kJ/mole, indicating that the removal of TBBPA by Cu/Fe BNPs is surface-control mechanism. For the effect of aqueous pH, TBBPA removal by Cu/Fe NPs favored acid and neutral conditions. The removal rate constant increased from 0.191 to 0.228 min^{-1} with the decrease of pH from 9.0 to 5.0. The removal rate constant decreased to 0.162 min^{-1} with continuously dropped the pH to

3.0. Besides, the removal efficiencies were over 98.5 % and have no obvious difference at pH 3.0 to 9.0. However, at pH 11.0, the removal efficiency only 77.0 % with removal rate constant of 0.063 min^{-1}. The complete debromination pathways of TBBPA with Cu/Fe were also presented by the identified byproducts: tribromobisphenol A, dibromobisphenol A, bromobisphenol A, and bisphenol A (BPA). In principle, the removal of the final debrominated byproduct, BPA, can be degraded by Fenton reaction through residual iron ions and additional H_2O_2. In BPA solutions, the increase of either H_2O_2 or Fe^{2+} concentration increased the BPA removal rate. However, a higher concentration of H_2O_2 or Fe^{2+} (both are 2.5mM) cause the BPA removal rate constant drop from 0.015 min^{-1} to 0.0107 min^{-1} and from 0.015 min^{-1} to 0.0014 min^{-1}, respectively. The results demonstrated that our synthesized Cu/Fe bimetallic nanoparticles have a high potential for TBBPA treatment and combine with H_2O_2 to degrade most TBBPA debrominated byproducts effectively.

Keyword: tetrabromobisphenol A (TBBPA), bisphenol A (BPA), Cu/Fe bimetallic nanoparticles (Cu/Fe BNPs), debromination
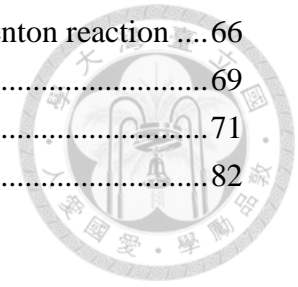
Tables of contents

List of Tables

List of Figures

Chapter 1 Introduction

For fire safety of products, brominated flame retardant (BFR) has been widely used in the world and is ubiquitous in many environmental media. Tetrabromobisphenol A (TBBPA) is a most-produced BFR. In order to meet safety standards, TBBPA is introduced into a variety of manufacturing polymer products with two kinds of forms: reactive (~90%) and additive form (Nakajima et al., 2009). Due to its volume of usage increasing as a replacement for banned BFRs and non-chemically bound, the additive form was suspected to release into environmental media (ECB, 2006; de Wit et al., 2010). A growing body of studies has confirmed that TBBPA has thyroid hormonal activity (Li et al., 2015; Covaci et al., 2009; Chan and Chan, 2012), neurotoxicity (Hendriks et al., 2012; Wojtowicz et al., 2014), cytotoxicity (Reistad et al., 2007; Ogunbayo and Michelangeli, 2007), hepatotoxicity (Szymanska et al., 2000; Ronisz et al.,2004), and it could cause immunological effects (Darnerud, 2003; Watanabe et al., 2010; Koike et al., 2013).

Many technologies have been used to remove TBBPA from the environment, such as chemical oxidation (Han et al., 2008; Lin et al., 2009; Qu et al., 2015), direct photolysis (Wang et al., 2015c), photocatalytic degradation (Xu et al., 2011), biodegradation (Ronen and Abeliovich, 2000; Chang et al., 2012), and chemical reduction (Liu et al.,2009; Lin et al., 2012). Particularly, for chemical reduction, zero valent iron (ZVI) has been widely used for treating many organic contaminants in contaminant sites (Song and Carraway, 2005; Puls et al., 1999). Furthermore, iron-based bimetallic nanoparticles were also capable of removing halogenated organic compounds with high efficiencies (Smuleac et al., 2011; Parshetti and Doong, 2012). When TBBPA was degraded via debromination (Luo et al., 2010; Huang et al.,

1

2013; Li et al., 2016), the TBBPA debrominated byproducts especially bisphenol A (BPA), which is an endocrine disruptor may cause negative effect in human bodies (Vom Saal et al., 2012). Fenton reaction could be a good method to degrade the TBBPA debrominated byproducts by only adding H_2O_2 with Fe^{2+} from iron oxidization (Moon et al., 2011; Li et al., 2013).

The aims of the research were to investigate following objectives:

1. To study the degradation of TBBPA by Cu/Fe bimetallic nanoparticles with various parameters (The effects of Cu loading, Cu/Fe dosage, TBBPA initial concentration, temperature and pH were carried out).

2. To study the mechanisms of the removal of TBBPA from water by Cu/Fe nanoparticles.

3. To study the removal of TBBPA debrominated byproducts by Fenton reaction.

Chapter 2 Literature Review

2.1 Introduction of tetrabromobisphenol A

Tetrabromobisphenol A (TBBPA) and its derivatives were a group of brominated organic compounds. Especially, TBBPA was the most-produced compound used as brominated flame retardant (BFR) with 58.8% bromine (de Wit et al., 2010), which was produced from bromination of bisphenol A (BPA). The size of the global TBBPA market was 170,000 tons in 2004 (George and Häggblom, 2008). TBBPA was accounted for 58.7 % of total world market demand of BFRs (BSEF, 2001). Table 2-1 gives the estimated annual market demand for the major BFRs for the years 2001–2003 (BSEF, 2006). TBBPA is introduced into manufacturing polymer applications in either a chemical bound reactive flame retardant (~90%) or an additive flame retardant (Nakajima, 2009). Reactive form was chemically bound to the material and thus do not migrate out of the material. TBBPA is also increasingly being used as an additive flame retardant in ABS plastics, as a replacement for banned BFRs (de Wit et al., 2010). A risk assessment has been performed within the European Union (EU), it concluded that, no health or environmental risks were identified when TBBPA is used in reactive form (EC, 2008). However, the risk of TBBPA degradation byproduct, bisphenol A and TBBPA derivative, dimethylated TBBPA had to further be certified. In addition, the risk assessment also concluded that there is a need for specific measures to limit risks when TBBPA is used as an additive flame retardant (EC, 2008). TBBPA had been found in various environments. Moreover, many studies have confirmed that TBBPA can cause many diseases, including immunotoxicity (Pullen et al., 2003), neurotoxicity (Viberg and Eriksson, 2011), disruption of thyroid homeostasis (Meerts et al., 2000; Kitamura et al., 2002), cytotoxicity

3

(Decherf et al., 2010) and hepatotoxicity (Szymanska et al., 2000). Therefore, developing an effective method to remove TBBPA from environments is essential. Figure 2-1 shows the structure of TBBPA.

Table 2-2 shows the chemical and physical properties of TBBPA. TBBPA (CAS No. 79-94-7) is a crystalline solid. The chemical formula is $C_{15}H_{12}Br_4O_2$. The melting point and the boiling point of TBBPA are 178 ^{o}C and over 200 ^{o}C, respectively. It is limited solubility in water, and previous reports determined the water solubility of TBBPA at neutral condition is between 0.24-4.16 mg/L (GC, 2013; U.S. EPA, 2015) and it depends on pH (Han, 2008). The pK_a values for TBBPA are 7.5 and 8.5 (EFSA, 2011), indicating that it is a neutral compound in a neutral condition and the water solubility increases as pH increases (Nollet, 2011).

Table 2-1 Estimated annual worldwide market demand of BFRs in 2001 by region, and total estimated demand in 2002 and 2003 (metric tons) (BSEF[a], 2006).

	PentaBDE	OctaBDE	DecaBDE	TBBPA	HBCD
Americas[b]	7,100	1,500	24,500	18,000	2,800
Europe	150	610	7,600	11,600	9,500
Asia	150	1,500	2,300	89,400	3,900
Total (2001)	7,500	3,790	56,100	119,700	16,700
Total (2002)	-	-	65,700	150,600	21,400
Total (2003)	-	-	56,400	145,100	22,000

[a] *BSEF* was an abbreviation of *Bromine Science and Environmental Forum.*

[b] Americas includes North and South America, but North America, particularly the USA, is the major user.
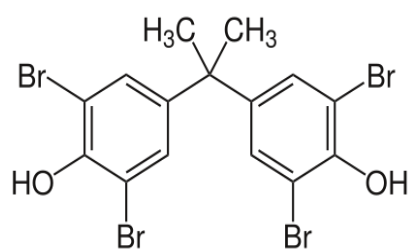
Figure 2-1 The structure of TBBPA.

Table 2-2 Physical-chemical properties of TBBPA (Adapted from USEPA, 2015)

Property	Statement and value
CAS No.	79-94-7
Color	Powder white or colorless
Chemical formula	$C_{15}H_{12}Br_4O_2$
Molecular mass (g/mol)	543.88
Melting point (℃)	178
Boiling point (℃)	>200
Density (g/cm^3)	2.12
Water solubility (mg/L)	0.24[a]-4.16[b]
Vapor pressure (mm Hg)	$<1x10^{-6}$
pKa	7.5/8.5
Log K_{ow}	4.5[c]-9.7[d]
Log K_{oc}[e]	5.4
Henry's law constant[a]	$<1.0 \times 10^{-10}$ atm · m^3/mole

[a] European Union (EU) (2012)

[b] Li et al. (2015) and Kuramochi et al.(2008)

[c] WHO (1995) and Kuramochi et al.(2008)

[d] Zhang et al. (2015)
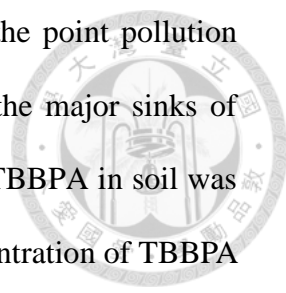
[e] USEPA (2015)

5

2.2 The fate of TBBPA in the environment

TBBPA has been detected in various environmental media (Sun et al., 2014) since it would possible release into the environment from source during manufacture, utilization, and disposal (such as recycling, incineration and deposit at landfill) of TBBPA-containing products. Because TBBPA is manufactured in bulk mass production and used widely for many artificial products, TBBPA is widespread in the world. For example, there are many disposals of electronic wastes (e-wastes), in which a large number of TBBPA were addicted and peripheral equipment during the manufacturing process. U.S. EPA released toxics release inventory (TRI) report to indicate that 52 manufacturing and processing facilities released or disposed approximately 127,845 pounds of TBBPA (U.S. EPA, 2015). TBBPA would be persistent in a variety of environmental media. In fact, TBBPA has been detected in various environmental media including soil (Huang et al., 2014; Matsukami et al., 2015), sediment (Wang et al., 2015a; He et al., 2013), sewage sludge (Gorga et al., 2013; Morris et al., 2004), water (Harrad et al., 2009; Osako et al., 2004), dust (Zhou et al., 2014; Wang et al., 2015b), air (Ni and Zeng, 2013; Liu et al., 2016), and even biota samples (Cariou et al., 2008; Johnson-Restrepo, 2008).

TBBPA could transport from environment via various sources and exposure pathways. The important sources of TBBPA are its chemical manufacturing, processing and consumer product use. In chemical manufacturing and processing, dust (unintended exposure from incidental ingestion of inhaled particles/dust), diet (Soil/plants/livestock), and fish ingestion (surface water and sediment) were main exposure pathways. For consumer product use, products and indoor dust were major pathways. Especially, young children are likely to exhibit higher exposure than older children and adults due to their more prevalent object-to-mouth behavior (USEPA,

6
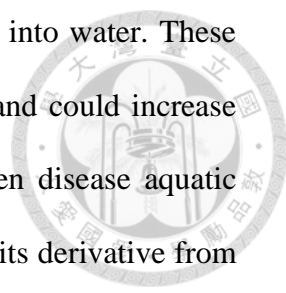
2015). Huang et al. (2014) also reported that the areas far from the point pollution sources were contaminated by fly ash deposition. Soil is one of the major sinks of TBBPA in the environment (Li et al., 2015). The concentration of TBBPA in soil was detected with 220 ng/g (Huang et al., 2014). However, a high concentration of TBBPA has been reported as 450 mg/kg in contaminated soil (Ronen and Abeliovich, 2000). In soil, under anoxic conditions, TBBPA is mainly finally reduced to bisphenol A (BPA) (Liu et al., 2013); Under oxic condition, TBBPA can be *O*-methylated to form its mono- and dimethyl ethers (MeO-TBBPA and diMeO-TBBPA, respectively) (George et al., 2008). BPA, MeO-TBBPA and diMeO-TBBPA have negative effect for some organisms (McCormick et al., 2010; USEPA, 2015). These O-methylated derivatives are more lipophilic and more persistent in the environment than the parent compound (Sun et al., 2014), which could cause more problems with more difficult to treat these compounds. TBBPA has been found in human bodies (blood, breast milk and adipose tissue) (Cariou et al., 2008; Shi et al., 2013; Johnson-Restrepo et al., 2008) and in biota (aquatic and terrestrial organisms) (Johnson-Restrepo et al., 2008; Yang et al., 2012). Additionally, it could cause many diseases in human bodies (Kitamura et al., 2002; Viberg and Eriksson, 2011).

In Taiwan, TBBPA is not a major chemical for environmental monitoring and few reports available (Ren, 2010). Most TBBPA pollution sources are chemical manufactory, but there is no TBBPA manufactory in Taiwan. All TBBPA chemicals in Taiwan are imported.

2.3 Effects of TBBPA in biota

2.3.1 Effect in aquatic organisms

TBBPA from manufacturing facilities could be disposed into the water;

7

furthermore, TBBPA in soil and sediment could leach and release into water. These pathways made the concentration of TBBPA in water increasing and could increase its exposure concentration and the opportunity to poison and even disease aquatic organisms. Plants have a high potential to accumulate TBBPA and its derivative from the soil (Sun et al., 2014). Sun et al. (2008) studied the uptake of TBBPA in coontail *Ceratophyllum demersum* L., and the result showed that TBBPA can be accumulated in plant in a large amount of 1.213 mg/g dry weight with exposure to 1.0 mg/L in 14 days. With exposure concentration and exposure time increasing, the production of reactive oxygen species (ROS) could be induced. It indicated that a significant damage which may occur in plants for TBBPA exposure. Moreover, several reports said that TBBPA was toxic to several aquatic invertebrates at low concentrations (USEPA, 2015). The EC_{50} value of 0.96 mg/L was determined by the experiment of acute exposure to TBBPA for freshwater aquatic invertebrates (*Daphnia magna*) (Waaijers et al., 2013). TBBPA caused lethality in the marine invertebrate species *Acartia tonsa* at a concentration of 0.40 mg/L (Wollenberger et al., 2002). Mussel (*Mytilus edulis)* reduced the shell length with a maximum acceptable toxicant concentration (MATC) of 0.023 mg/L was observed in a 70-day study (ACC, 2005). For sediment-dwelling worms, emergent insects and amphipods, the available sediment toxicity studies exhibited in the range of 117 - 500 mg/kg for the species tested. (USEPA, 2015; Krueger, 2002a, 2002b; ACC-BFRIP, 2006). Amphipods (*Hyalella azteca*) were exposed to TBBPA, resulting in the MATC of 354 mg/kg dry weight (ACC-BFRIP, 2006). Furthermore, acute toxicity studies were tested for a variety of fish species resulted in 96-hour LC_{50} values ranging from 0.40 to 1.1 mg/L (Table 2-3, GLCC,1978b,1988a).

8

Table 2-3 Toxicity of TBBPA to fish (U.S. EPA, 2005)

Test Organism	Fresh/ Salt Water	Test Guideline/ Study Type	Duration	Endpoint	Concentration (mg/L)	Chemical Analysis	Effects	Reference
Rainbow trout *Oncorhynchus mykiss*	Fresh	OECD TG 203, 1984	96-hr	LC50	0.40	Nominal	Mortality	GLCC (1978b)
Bluegill sunfish *Lepomis macrochirus*	Fresh	OECD TG 203, ASTM, 1975	96-hr	LC50	0.51	Nominal	Mortality	GLCC (1978a)
Fathead minnow *Pimephales promelas*	Fresh	OECD TG 203, 1984	96-hr	LC50	0.54	Measured Flow-through	Mortality	GLCC (1988a)
Rainbow trout *Oncorhynchus mykiss*	Fresh	OECD TG 203	96-hr	LC50	1.1	Measured Flow-through	Mortality	ACC (2003)
Zebra fish *Danio rerio*	Fresh	OECD TG 202	96-hr	LC50	1.1	Nominal Static	Mortality	Chow et al. (2013)

2.3.2 Effect in terrestrial organisms

TBBPA reached to the terrestrial environment because of human activities, e.g. sewage sludge amendment, and natural dispersion. Wang et al. (2016) first demonstrated that rice cell suspension culture could accumulate and metabolize TBBPA. Moreover, the MATC of five plant species have been determined as 518, 32, 518, 127 and 518 mg/kg dry soil for corn, cucumber, onion, ryegrass and tomato, respectively (ACC-BFRIP, 2002). For soil invertebrate toxicity, an earthworm study was carried out and using reproduction as the endpoint (Sverdrup et al., 2006). Exposing the earthworm (*Enchytraeus crypticus)* to TBBPA for 21 days, the lowest observed effect concentration and MATC were 10 and 5.5 mg/kg soil (dry weight), respectively (Sverdrup et al., 2006). Halldin et al. (2001) concluded that TBBPA's transfer to the embryo from the yolk was low with rapid metabolism and excretion by the experiment that TBBPA was injected to quail yolk to evaluate its distribution and the potential for certain reproductive and endocrine effects in adult birds. TBBPA exposure in amphibians might cause adverse effects on the endocrine system (Brown

et al., 1996; Hanada et al., 2003; Kashiwagi et al., 1999), in other words, TBBPA changed the normal thyroid hormone-mediated gene expression (Veldhoen et al., 2006).

2.3.3 Bioaccumulation of TBBPA

The $logK_{ow}$ of TBBPA is 4.5-9.7. Based on its the high $logK_{ow}$, TBBPA was expected to have a great potential for accumulating in biota. Nevertheless, there are two different results have been reported. One result reported that TBBPA has low bioaccumulation potential (Colnot et al., 2014; USEPA, 2015), and the other result showed the high potential bioaccumulation for TBBPA. Tao et al. (2016) measured the bioaccumulation factor (BAF) of TBBPA in mud carp and Chinese mystery snail in electronic waste site, about 2500 and 5190, which were very high. Szymanska et al. (2001) also observed high concentrations of TBBPA in many tissue of Rat. The bioaccumulation of TBBPA is tissue-specific and species-specific (Tang, 2015).

2.3.4 Human hazard potential

There are two different results for TBBPA's human hazardous potentials reported. Some reports from U.S. EPA and European Union concluded that no health hazards of potential concern to adults (U.S. EPA; EC, 2006). However, the data were not very clear and many available reports data were collected from adult animal experiment. On the contrary, the toxicity of TBBPA for newborns and adolescents has been paying attention in recent years. Fukuda et al. (2004) said that exposing to TBBPA caused slight kidney lesions at 200 mg/kg-bw/day in newborn rats and it was possibly due to immature metabolic capability. Tada et al. (2006) found very slight hepatocyte necrosis in offspring of female mice exposed to TBBPA at 140.5

mg/kg-bw/day during gestation through weaning of the offspring.

2.4 Introduction of zero valent iron and bimetallic particles

2.4.1 Microscale zero valent iron

For treatment of organic compounds and heavy metal contaminants, the utilization of zero valent metals including iron (Fe^0), zinc (Zn^0) (Wang et al., 2008; Choi and Kim, 2009), aluminum (Al^0) (Bokare and Choi, 2009; Lien et al., 2010; Liu et al., 2011), and copper (Cu^0) (Huang et al., 2012; Raut et al., 2016) has received significant attention because of suitable redox potential, high reactivity, and effective cost. Zero valent iron (ZVI, Fe^0) is one kind of metals that has been extensively studied and widely applied for treatment of environmental contaminants. It was well known for its high potential application in decomposition of halogenated organic compounds (Lowry and Johnson, 2004; Eggen and Majcherczyk, 2006)

According to Table 2-4, the standard electrode potential of Fe^{2+}/Fe^0, -0.44 V (Eq. 2-1) (Bratsch, 1989), indicated Fe^0 is a strong reductant. Alky halides (RX) were electronegative and their standard electrode potentials generally in the range from +0.5 to +1.5 V at pH 7 (Eq. 2-2) (Vogel et al., 1987). O_2 is a strong oxidant and its standard electrode potential is +1.23 V (Eq. 2-3). The Fe^{2+} and H_2 could be produced and play a role of reducing agent during the ZVI reduction reaction in aqueous solutions. The standard electrode potential of H_2O in Eq. 2-4 was -0.83 V. Fe^{2+} has the standard electrode potential of +0.77 V (Eq. 2-5).

Table 2-4 The standard electrode potentials of various elements for aqueous solutions at 25 °C.

Equation	Standard electrode potential (V)	
$Fe^{2+} + 2e^- \rightarrow Fe^0$	-0.44	(2-1)
$RX + 2e^- + H^+ \rightarrow RH + X^-$	+0.50 - 1.5	(2-2)
$O_2 + 4e^- + 2H_2O \rightarrow 4OH^-$	+1.23	(2-3)
$2H_2O + 2e^- \rightarrow H_2 + 2OH^-$	-0.83	(2-4)
$Fe^{3+} + e^- \rightarrow Fe^{2+}$	+0.77	(2-5)
$Fe^0 + O_2 + 2H^+ \rightarrow Fe^{2+} + H_2O$	+0.70	(2-6)

In the reaction, three reductants (iron metal, ferrous ion and hydrogen) in the solution according to the theory of electrochemistry suggested three pathways in the system (Matheson and Tratnyek, 1994; Scott Orth and Gillham, 1996) (Figure 2-2). First, Fe^0 transfers electrons from its surface to the alkyl halide that is adsorbed on the Fe^0 surface and served as the oxidizing agent by reductive dehalogenation (Eq. 2-7) (Matheson and Tratnyek, 1994). Peng et al. (2013) also reported that polybrominated diphenyl ethers were removed by MZVI through adsorption and debromination in a sequential step.

$$Fe^0 + RX + H^+ \rightarrow Fe^{2+} + RH + X^- \tag{2-7}$$

Second, the ferrous iron (Fe^{2+}) was a reductant with the ability to reductively dehalogenate alkyl halides (Eq. 2-8). Under an anaerobic condition, Fe^0 reacted with water to produce Fe^{2+} (Eq. 2-9), moreover, when dissolved O_2 present, Fe^{2+} could be also produced (Eq. 2-10). Both reactions caused that the pH increased and the iron

hydroxide (Fe(OH)$_2$) precipitated (Eq. 2-11) (Figure 2-3). Fe(OH)$_2$ was rapidly oxidized to Fe(OH)$_3$, which might form a surface layer on the iron and result in passivation, for this reason, the Eq. 2-8 would be limited.

$$2Fe^{2+} + RX + H^+ \rightarrow 2Fe^{3+} + RH + X^- \qquad (2\text{-}8)$$

$$Fe^0 + 2H_2O \rightarrow Fe^{2+} + H_2 + 2OH^- \qquad (2\text{-}9)$$

$$Fe^0 + O_2 + H_2O \rightarrow 2Fe^{2+} + 4OH^- \qquad (2\text{-}10)$$

$$Fe^{2+} + 2OH^- \rightarrow Fe(OH)_2 \qquad (2\text{-}11)$$
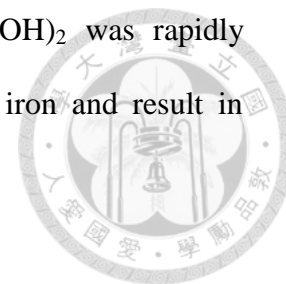
Third, hydrogen involved in the reductive halongenation of alkyl halides which was produced as a product of corrosion with H$_2$O (Eq. 2-12).

$$H_2 + RX \rightarrow RH + H^+ + X^- \qquad (2\text{-}12)$$

In addition to reductive reaction, Fe^0 could also drive oxidative reactions in the presence of hydroxyl radicals (HO ·) that produced by Fe^{2+} collide with hydrogen peroxide (H$_2$O$_2$) (Eq. 2-13). Eq. 2-13 has been called as Fenton reaction. (Bremner et al., 2006; Hseh et al., 2005). H$_2$O$_2$ could be generated according to the reduction of O$_2$ occurring on Fe^0 surface (Eq. 2-14) (Lv et al., 2016). Hydroxyl radicals were induced by Eq. 2-13. The Fenton reaction was also carried out in Fe^0-H$_2$O system.

$$Fe^{2+} + H_2O_2 \rightarrow Fe^{3+} + HO · + HO^- \qquad (2\text{-}13)$$

$$Fe^0 + O_2 + 2H^+ \rightarrow Fe^{2+} + H_2O_2 \qquad (2\text{-}14)$$

For Fe^0-H$_2$O system, the electron transfer on Fe^0 surface could precede both reductive

13

and oxidative reactions.
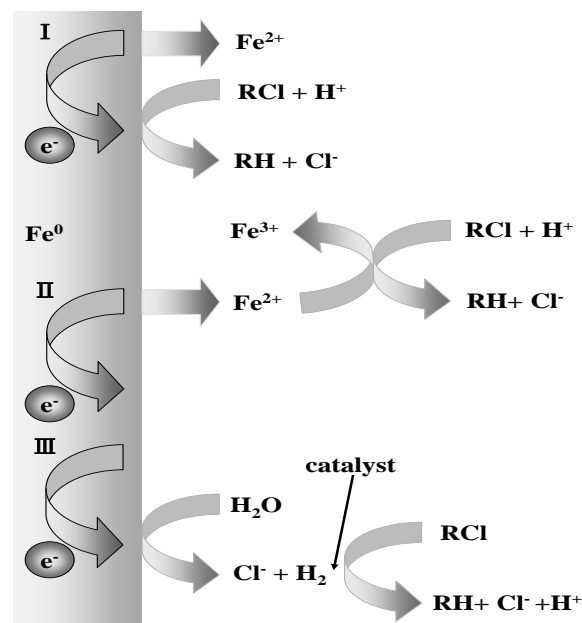
Figure 2-2 Proposed pathways for reductive dehalogenation in anoxic Fe-H_2O system (Matheson and Tratnyek, 1994).
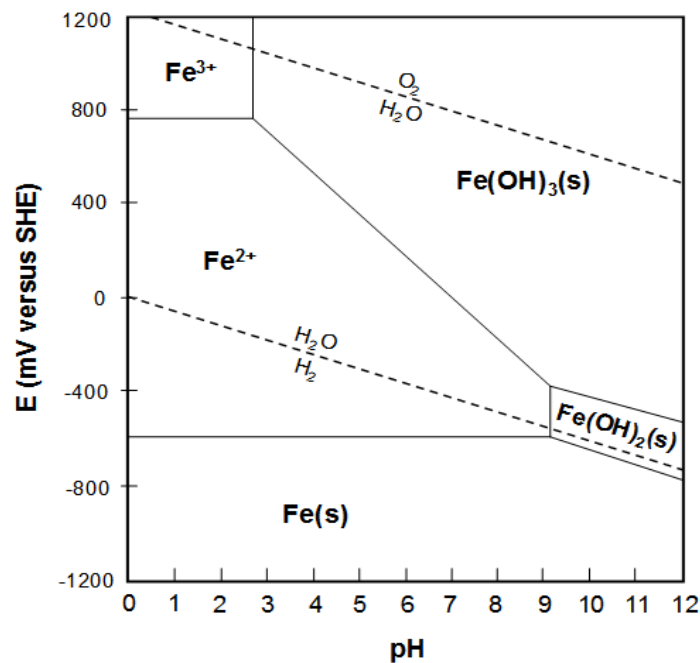
Figure 2-3 The pH-Eh diagram for iron oxides and hydroxides at 25 $^{\circ}$C (Stumm and Morgan, 1981).

14

2.4.2 Nanoscale zero valent iron

In recent years, nano zero-valent iron (NZVI) technology has received lots of attentions and increasingly employed for removing contaminants such as reductive dehalogenation of halogenated organic contaminants (Lv et al., 2016; Fu et al., 2014; Yan et al., 2013). More and more studies with NZVI have focused on halogenated aliphatic compounds and even persistent halogenated aromatic contaminants. It has been suggested to increase removal efficiency due to its good adsorptive and reactive characteristics with huge specific surface area and high volume ratio (Yan et al., 2010; Xiu et al., 2010).

2.4.3 Iron-based bimetallic nanoparticles

In recent years, many iron-based bimetallic particles have been synthesized and investigated to eliminate environmental contaminants because of the shortcomings of NZVI that decreased reactivity during reaction. For previous studies, NZVI has very slow reaction rates for catalyzing dehalogenation of halogenated compounds (Wang and Zhang, 1997; Zhuang, 2011). In order to improve the dehalogenation efficiency, secondary metal as a catalyst has been incorporated with NZVI to form bimetallic particles (Kim and Carraway, 2000; Zhuang, 2011; Luo, 2011). Secondary metals such as Pt, Pd, Ni, Cu, and Ag have standard electrode potential (E^0) more positive than Fe^0, which may be reduced by NZVI to form bimetallic nanoparticles (Pt^0/Fe^0, Pd^0/Fe^0, Ni^0/Fe^0, Cu^0/Fe^0 and Ag^0/Fe^0) (Table 2-5) (O'Carroll et al., 2013). The activation energy of the reaction could be lowered when the addition of a second metal, allowing more interactions between the compounds to result in reactions, thus increasing the reaction rate (O'Carroll et al., 2013). Li et al. (2006) reported that second metal can prevent oxidation when the particles are exposed to

15

air; moreover, it can inhibit the formation of an oxide layer that passivated the reactive sites of NZVI (Lien and Zhang, 2001). The incorporation of the catalytic metal made it have a higher surface area and increase the number of reactive sites on the iron surface (Bokare et al., 2007; Shao-ping et al., 2005). Several reports reported that proton and water could be reduced to atomic and molecular hydrogen at the surface of second metal, and make further hydrogenation of halogenated organic compounds (Bokare et al., 2007; Gui et al. 2000). The introduction of second metal also enhanced the formation of hydride on the surface and acted as the reducing agent for halogenated compounds; thus facilitating the transfer of electrons and atomic hydrogen to the contaminants (Bokare et al., 2007; Lien and Zhang, 2007; Lin, 2012).

The bimetallic nanoparticles could serve as strong electron donors and involve the transfer electrons to the organic contaminants, and then reduce them with a trace amount of second metal as catalyst under anaerobic condition (Joo and Zhao, 2008). For treatment of halogenated organic contaminants, the dehalogenation has been viewed as rate-determining step. For dehalogenation, the C-H bond formation after the carbon-halogen bond (C-X) was broken, thus, halogen was replaced with hydrogen by the electron transfer from NZVI to secondary metal (Schrick et al., 2002).

Yan et al. (2013) illustrated reaction mechanisms for TCE reduction by nZVI and Pd-nZVI with a prposed model (Figure 2-4). It showed that a synergistic effect between the second metal (e.g. Pd) and Fe, whereby Pd serves as the hydrodehalogenation and hydrogenation catalyst and Fe provides the hydrogen source through water reduction.

Table 2-5 Standard redox potentials (E^0) in aqueous solution at 25 ℃

Aqueous solution	Half reactions	E^0 (V)
Platinum (Pt)	$Pt^{2+} + 2e^- \leftrightarrow Pt$	1.19
Palladium(Pd)	$Pd^{2+} + 2e^- \leftrightarrow Pd$	0.92
Silver (Ag)	$Ag^+ + e^- \leftrightarrow Ag$	0.80
Copper (Cu)	$Cu^{2+} + 2e^- \leftrightarrow Cu$	0.34
Nickel (Ni)	$Ni^{2+} + 2e^- \leftrightarrow Ni$	−0.25
Iron (Fe)	$Fe^{2+} + 2e^- \leftrightarrow Fe$	−0.44
Zinc (Zn)	$Zn^{2+} + 2e^- \leftrightarrow Zn$	−0.76
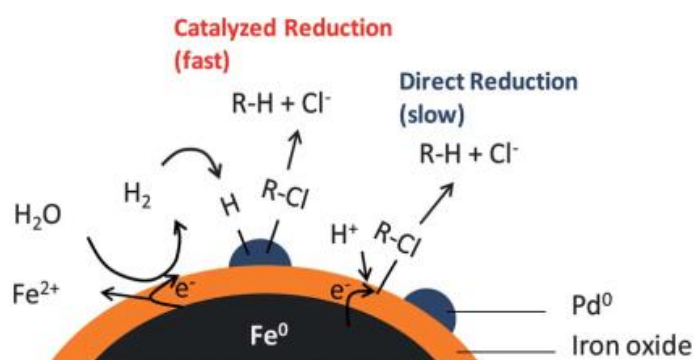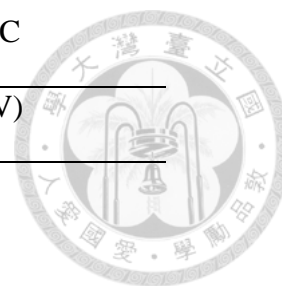
Figure 2-4 Mechanisms of reductive dechlorination by monometallic NZVI and palladium-doped nZVI (Yan et al., 2013).

2.5 The approaches of TBBPA removal

Due to extensive use and potential hazard for human of TBBPA, the development of effective methods to eliminate TBBPA is important. There are many techniques for TBBPA removal, such as photodegradation, biodegradation, and iron-based composite.

17

2.5.1 Biodegradation

Biodegradation is a well-known method that used to treat halogen organic compounds. Many environmental media contain microorganisms that are capable of dehalogenating compounds like polychlorinated biphenyls, polychlorinated phenols, and benzene, as well as many chlorinated solvents and brominated compounds (Ronen and Abeliovich, 2000; Shih et al., 2012). An et al. (2011) isolated a novel bacterium, *Ochrobactrum* sp. T, from an e-waste recycling site that was capable of simultaneous debromination and aerobic mineralization of TBBPA. Moreover, the level of oxygen influences the pathway and microorganism species of TBBPA biodegradation (Nyholm et al., 2010). Chang et al. (2012a, 2012b) isolated two kinds of bacteria from Erren river, which can perform aerobic or anaerobic degradation of TBBPA. However, biodegradation spend more time for contaminant removal than chemical degradation though it was eco-friendly and cost-effective.

2.5.2 Photodegradation

Wang et al. (2015) and Zhong et al. (2012) have studied the photolytic degradation of TBBPA degradation and indicated that it can be considered as a promising technique. In the photochemical reaction, reactive oxygen species (ROS) such as singlet oxygen ($^1O_2$) or the superoxide anion radical ($O_2 \cdot ^-$) were responsible for its degradation (Han et al., 2008). Besides, debromination is also a pathway of TBBPA photodegradation (Bao and Niu, 2015). Many composite materials also are used for photocatalytic oxidation of TBBPA, such as $Ag/Bi_5Nb_3O_{15}$ (Guo et al., 2011), BiOBr (Xu et al., 2011), and titanomagnetite (Zhong et al., 2012). Furthermore, Zhong et al. (2012) combined Fenton reaction and photodegradation to

18

obviously increase the TBBPA degradation.

2.5.3 NZVI and iron-based bimetallic nanoparticles

NZVI and iron-based bimetallic nanoparticles have the powerful ability to remove the halogen organic compounds that mentioned above. And many iron-based nanomaterial composite and modified BNP are studied for increasing the stability and reactivity of nanoparticles with a better efficiency to contaminant remediation (Doong et al., 2015; Lin et al., 2015). For TBBPA, Lin et al. (2012) investigated the debromination of TBBPA by NZVI in methanol/water (50/50) solutions with rate constant of 0.512 ± 0.057 h^{-1} at pH 7.5 and it shows that methanol/water ratio could influence the debromination of TBBPA. In short, in order to rapid decomposition of TBBPA, Fe-Ag and Fe-Ni bimetallic nanoparticles coupled with microwave energy were carried out (Luo et al., 2012). Luo et al. (2010) demonstrated that the TBBPA removal rate is 0.22 ± 0.02 min^{-1} with 0.4 g/L Fe–Ag bimetallic particles, Ag content = 1 wt.%, at an initial pH value of 6.0 ± 0.5 and initial temperature of 30 ℃ and the bottles were placed in ultrasonic wave shaker (40 kHz and 100 W) during the entire reaction period. Both Ag in catalyst and ultrasonication (US) play important roles in the activity of US/Fe–Ag system for TBBPA degradation. Huang et al. (2013) showed the kinetics of TBBPA and degradation byproduct removal with various pH (pH 4.2-7.2). The best fit k_{obs} values for the disappearance of TBBPA increased from 0.077 ± 0.005 to 2.60 ± 0.03 min^{-1} for the solution pH from 7.2 decreased to 4.2. Li et al. (2016) also indicated that the reaction of Ni/NZVI with TBBPA was a surface mediated reaction for the different results of EDS and XPS with Fe contents before and after the reaction. Though there are many studies use bimetallic nanoparticle such as Ni/Fe, Pd/Fe and Ag/Fe to treat halogenated organic

19

contaminants even TBBPA, few reports use Cu as a second metal. Most bimetallic particles with Cu as second metal were not used iron as a based metal, and alumium and zinc are common metals (Huang et al., 2015). Researcher used Cu/Fe bimetallic to treat halogenated organic contaminants such as HCB (Zheng et al., 2009; Zhu et al., 2010) but TBBPA was not a target compound.

2.5.4 Fenton reaction

Fenton reaction is an advanced oxidation process and well studied for treating organic compounds, such as dyes (Moon et al., 2011; Lucas et al., 2006), phenol (Yalfani et al., 2009; Jiang et al., 2010), and halogenated compounds (Chamarro et al., 2001; Xu and Wang, 2011). Fenton's reagent is a mixture of H_2O_2 and ferrous iron. Under acidic conditions, it generated hydroxyl radical in the reaction (Neyens and Baeyens., 2003). The overall reaction is:

$$H_2O_2 + Fe^{2+} \rightarrow Fe^{3+} + HO^- + HO \cdot$$
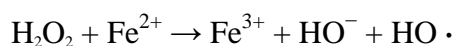
The hydroxyl radical is a strong oxidant that can oxidize many recalcitrant organic compounds rapidly (Zhou et al., 2008). In order to enhance the removal efficiencies of recalcitrant organic compounds, many modified Fenton reactions have been suggested by researchers, such as sono-Fenton (Wang and Shih, 2015), electron-Fenton (Pimental et al., 2008), and photo-Fenton (Lucas and Peres, 2006). Besides, a sequential process with pretreatment by ZVI and then Fenton reaction for dye (Shih and Tso, 2012) was proposed to be an effective method for contaminant removal by using ferrous/ferric ions from the oxidation of ZVI.

Chapter 3 Material and methods

3.1 Chemicals

Ferrous sulfate heptahydrate (FeSO$_4 \cdot$ 7H$_2$O, 99.5-102 %) was purchased from Merck. Sodium borohydride (NaBH$_4$, 95 %) and sodium bicarbonate (NaHCO$_3$, 99.7 %) were obtained from Riedel-deHaen. Copper sulfate pentahydrate (CuSO$_4 \cdot$ 5H$_2$O, 99-102 %), nickel sulfate hexahydrate (NiSO$_4 \cdot$ 6H$_2$O, 99 %), ammonium acetate (CH$_3$COONH$_4$, 98%) and 1,10-phenanthroline hydrochloride (C$_{12}$H$_8$N$_2 \cdot$ HCl, 98%) were purchased from Sigma-Aldrich. Acetic acid (CH$_3$COOH, 100 %), hydrogen chloride (HCl, 36.5-38.0 %), sodium hydroxide (NaOH, 98.7 %), sodium carbonate (Na$_2$CO$_3$, 98 %), and sodium phosphate (Na$_2$HPO$_4$, 99.1 %) were obtained from J. T. Baker. All solvents (hexane and methanol) were ultra resi-analyzed grade and purchased from Burdick and Jackson. All aqueous solutions were prepared by using pure water, deionized with Milli-Q water purification system (18.2 MΩ/cm, Mill pore, Bedford, MA, USA).

 Tetrabromobisphenol A (TBBPA, 98%) was obtained from Aldrich. Bisphenol A (BPA, 97%) and hydrogen peroxide (H$_2$O$_2$, 35wt. %) were purchased from Acros. Stoke solutions of TBBPA and BPA were stored at 4℃ in the dark, and let them reach to room temperature before use.

3.2 Synthesis of NZVI, Ni/Fe, and Cu/Fe nanoparticles

Nanoscale zero valent iron particles were produced by the modified procedure from Wang and Zhang (1997) with adding 1.6 M NaBH$_4$ aqueous solution dropwise to a flask containing 1.0 M FeSO$_4 \cdot$ 7H$_2$O aqueous solution at ambient temperature.

21

Ferrous ion was reduced by borohydrate and zero valent iron particles precipitated instantly according to the following reaction:

$$Fe(H_2O)_6{}^{2+} + 2BH_4{}^- \rightarrow Fe^0\downarrow + 2B(OH)_3 + 7H_2\uparrow \qquad (3\text{-}1)$$
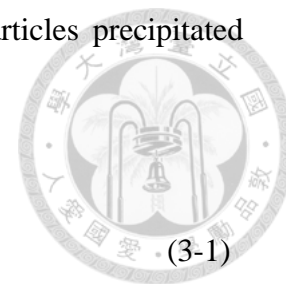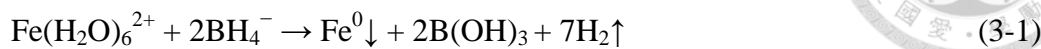
Nanoscale Bimetallic Cu/Fe particles were prepared by the deposition of desired amount of Cu^{2+} on NZVI with adding the copper sulfate aqueous solution into synthesized NZVI under a stirring condition according to the following equation:

$$Cu^{2+} + Fe(s) \rightarrow Cu(s) + Fe^{2+} \qquad (3\text{-}2)$$

After that, the Cu/Fe nanoparticles were filtered through a 0.22 μm membrane filter and washed with deoxygenated ultrapure water for several times. Subsequently, the Cu/Fe nanoparticles suspend in aqueous solution. Nanoscale bimetallic Ni/Fe particles were prepared with the same method of Cu/Fe preparation.

To check the effect of oxygen on the Cu/Fe nanoparticle synthesis, the removal reactions of TBBPA were evaluated by using Cu/Fe nanoparticles synthesized in a strictly anaerobic glovebox (Coy Laboratory Products Inc., USA) and in the atmosphere, respectively. To evaluate the oxidation of NZVI by copper (II), the oxidation states of iron before and after Cu ions adding were investigated.

3.3 Characterization of the synthesized Cu/Fe nanoparticles

The surface morphologies and physicochemical properties of the nanoparticles were characterized by field-emission scanning electron microscope with energy-dispersive X-ray spectroscopy (FE-SEM-EDS) and transmission electron

microscope (TEM). The particle size was determined by dynamic light scattering (DLS). The surface area was analysis by using Brunauer-Emmett-Teuller (BET) N_2 adsorption method. The crystalline phase of Cu/Fe nanoparticles was identified with X-ray diffraction (XRD). The relative oxidation state of Cu/Fe nanoparticles was analyzed using X-ray absorption near edge structure (XANES).

3.3.1 Field-emission scanning electron microscope, FE-SEM

The SEM imagines of nanoparticles were obtained using JEOL JSM-7600F scanning electron microscope (JEOL, Japan) equipped with an energy dispersive X-ray (EDX) probe for semiquantitative chemical analysis. The accelerating voltage was 30 kV. The nanoparticles were separated from the suspension by vacuum filtration. The solid was filtrated through a 0.22 μm membrane filter and then washed with deoxygenated ultrapure water several times before vacuum freeze-drying.

3.3.2 Transmission electron microscope, TEM

The TEM images of nanoparticles were taken with JEOL JEM-1200EX transmission electron microscope (JEOL, Japan) at 120 kV. A drop of Cu/Fe bimetallic nanoparticles was placed on a Cu-grid to dry. Cu/Fe nanoparticles diluted in ethanol and ultrapure water were sonicated (40 kHz, 280W) for 1 min, respectively, before TEM analysis.

3.3.3 Dynamic light scattering, DLS

In aqueous systems, particle size and particle size distributions were determined by a DLS instrument (Zetasizer Nano ZS, Malvern, MA, USA) at 25 $^{\circ}$C and at a measurement angle of 173°. DLS instrument utilizes a laser beam at 633 nm to

determine the size by measuring the particles' Brownian motion of the sample in particle suspensions with the viscosity of water, 0.08872 poise, and refraction index of 1.330, the refraction index of iron, 2.86, and its adsorption coefficient of 0.1. The Cu/Fe particle suspensions diluted with methanol of same volume and then being sonicated (40 kHz, 280W) for 30 seconds before DLS analysis. DLS measurements were conducted by adding 1 mL of sample into a DLS plastic cell. NZVI suspensions were injected in folded capillary cells, and the electrophoretic mobility was measured using a combination of electrophoresis and laser Doppler velocimetry techniques. The intensity of autocorrelation functions was converted by the CONTIN algorithm to intensity-weighted particle hydrodynamic diameter distributions, assuming the Stokes-Einstein relationship for spherical particles.

3.3.4 Brunauer-Emmett-Teuller surface area

Cu/Fe nanoparticles were pre-dried with vacuum freeze-dryer. Nitrogen Brunauer-Emmett-Teuller adsorption isotherms of Cu/Fe nanoparticles were analyzed with a surface area analyzer (Micromeritics, ASAP-2010/C5-05, USA). The surface area can be determined from the corresponding N_2 adsorption/desorption isotherms.

3.3.5 X-ray diffraction, XRD

The crystalline phase of Cu/Fe nanoparticles was identified with X-ray diffraction (XRD). Selected wet samples were analyzed at BL 13A1 beam line at the national synchrotron radiation research center (NSRRC) of Taiwan, using bicron diffractometer with a wavelength of 0.1 Å adjusted with Si (111) monochromator. All samples were prepared and immersed in water in a plastic bag for XRD and the following XANES analysis. The nanoparticles were scanned from 5° to 35° (θ) with

24

step increments of 0.025° and time per step of two seconds. The radiation wavelength of data from the synchrotron were converted to Cu Kα radiation (λ=1.5418 Å) and as showed in Figure 4-5, the wavelength have been converted to Cu Kα radiation (λ=1.5418 Å).
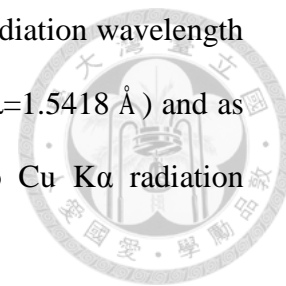
3.3.6 X-ray absorption near edge structure, XANES

The relative oxidation state of Cu/Fe nanoparticles was analyzed using X-ray adsorption near edge structure (XANES). XANES spectra were collected from BL 16A1 and BL 07C1 beamlines at the NSRRC in Taiwan. The BL16A1 beamline was used to determine the oxidation state of iron only. The electron storage ring was operated with energy of 1.5 GeV and current of 300 mA. A Si(111) double-crystal monochromator (DCM) was used to provide highly monochromatized photon beams with energies of 2 to 8 keV and an energy resolution of 1.5×10^{-4} ~ 2.1×10^{-4} (keV/keV). The BL 07A1 beamline was used to determine the oxidation states of copper. The electron storage ring was also operated the same as above. A Si (111) DCM was also used to provide highly monochromatized photon beams with energies of 5 to 23 keV and an energy resolution of 1.5 ~ 2.5×10^{-4} (keV/keV). The data were collected in fluorescence mode with a Lytle ionization detector in the region of the Fe K edge (7115 eV) and Cu K-edge (8979 eV) at room temperature. The K-edge XANES scans for Fe (6912-7512 eV) and Cu (8779-9379 eV) were recorded with step increments of 0.2 eV and 4.0 eV, respectively. The XANES data were then analyzed by Athena version (0.8.058). To keep the samples in a reduction condition, solid particles were prepared in glovebox with ethanol and saved in plastic bags before put in the box that was full of CO_2. After squeeze out the solid particles samples on the tapes, and then the samples were analyzed immediately.

25

3.3.7 Raman spectroscopy

The home-bult confocal Raman microscope is equipped with a monochromator (Shamrock SR 303i-A, Andor Technology, USA), a He-Ne laser (25-LHP-928-249, CVI Melles Griot, USA), a thermos- electric cooling CCD (DU 401-BR-DD-968, Andor, USA) and a microscope (BX51, Olympus, Tokyo, Japan). The sample of Raman spectroscopy were placed on a stainless steel holder and analyzed.

3.4 Batch experiments

The batch removal experiments for TBBPA transformation were conducted under Cu/Fe system in 4 ml amber glass vials capped with Teflon-lined septa under different environmental conditions. The removal was initiated by mixing 15 µL of a tetrabromobisphenol A stock solution (1000 mg/L) which was prepared by dissolved TBBPA powder in methanol and a certain amount of freshly prepare Cu/Fe nanoparticles suspension as depicted in the following experiments. The total reaction volume was 3 mL and the reactors were shaken continuously at 150 rpm for the duration of experiments at 25 ± 2 ℃. Each experiment was carried out triplicate. Control experiments were carried out identically except for the addition of Cu/Fe nanoparticles suspension.

3.4.1 The effects of Cu content and Cu/Fe dosage on the removal of TBBPA with Cu/Fe nanoparticles

For Cu/Fe nanoparticle system, the batch experiments were performed to investigate the effect of Cu contents (0.5, 2.0, 4.0, 8.0 %) and Cu/Fe dosage (1.0, 2.0, 3.0, 4.0 g/L) on the removal of TBBPA with Cu/Fe nanoparticles. The initial concentration of TBBPA was 5 mg/L at room temperature (about 25 ± 2 ℃) and the

pH were not further adjusted (about pH 6.8-7.1).

3.4.2 The effect of TBBPA concentration on the removal of TBBPA with Cu/Fe nanoparticles

The effect of initial TBBPA concentrations (1.0, 5.0, 10.0, 15.0 mg/L) on the removal of TBBPA with Cu/Fe nanoparticles was studied by the batch experiments. The dosage of Cu/Fe was 2.0 g/L containing 4.0 % Cu content, the initial pH value was 6.8 and the temperature was 25 ℃.

3.4.3 The effect of initial pH on the removal of TBBPA with Cu/Fe nanoparticles

For Cu/Fe nanoparticles system, the batch experiments to investigate the effects of initial pH of pH 3.0, 5.0, 7.0, 9.0 and 11.0 on the removal of TBBPA by Cu/Fe nanoparticles. Initial solution pH was controlled by hydrochloric acid and sodium hydroxide. Buffers were not used to avoid complications from buffer-metal interactions. The pH values were monitored by pH meter with time. The initial concentration of TBBPA for removal reactions was 5 mg/L, the Cu/Fe dosage was 2.0 g/L containing 4.0 % Cu content for each experiment and the temperature was 25 ℃. The concentrations of TBBPA in the aqueous and solid phases were analyzed as 3.5.1 mentioned.

3.4.4 The effect of initial temperature on the removal of TBBPA with Cu/Fe nanoparticles

The effect of temperature on the removal of TBBPA with Cu/Fe nanoparticles

27

was conducted under different temperatures. The temperature was controlled in a shaking bath at the desired temperatures of 5, 15, 25, 35, and 45 ℃. The initial concentration of TBBPA was 5 mg/L, the Cu/Fe dosage was 2.0 g/L containing Cu content of 4.0 %, and the initial pH value about 6.8.
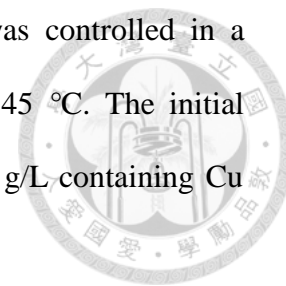
The Arrhenius equation can be used to determine the activation energy for the reaction.

$$k = Ae^{(-Ea/RT)} \tag{3-3}$$

where k (min^{-1}) is the measured rate constants, A (L min^{-1} m^{-2}) is the frequency factor, E_a (kJ mol^{-1}) is the activation energy for the reaction, R (kJ K^{-1} mol^{-1}) is the ideal gas constant, and T (K) is the absolute temperature (Laidler, 1984).

3.4.5 Effects of the Fenton process

For H_2O_2-Fe^{2+} system, the batch experiments were carried out to study the effect of H_2O_2 on the removal of TBBPA debrominated byproduct with advanced oxidation. The efficiency of TBBPA debrominated byproduct removal by the Fenton's reaction was investigated by evaluating the effects of H_2O_2 and Fe^{2+} concentration on BPA removal.

The reaction solutions were composed of 5 mg/L BPA and selected H_2O_2 and Fe^{2+} concentration. The pH was adjusted by adding 0.1 M NaOH or 0.1 M HCl solution. The concentration of BPA and total organic carbon (TOC) were analyzed as mentioned in 3.5.4 and 3.5.7, respectively.

3.5 Analysis methods of TBBPA and its byproducts

3.5.1 TBBPA and BPA stock solutions

TBBPA and BPA solutions were prepared by dissolving a known mass of TBBPA and BPA powder in methanol as the stock solutions and stored at 4 $^{\circ}$C.
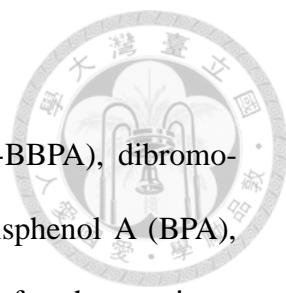
3.5.2 Extraction method of TBBPA in solid and aqueous phase

At the select time, the samples were conducted to determine the concentration of TBBPA on Cu/Fe surface and aqueous solutions after precipitation of Cu/Fe nanoparticles with magnet. Aliquots in aqueous phase were withdrawn and the concentrations of TBBPA analyzed by a high performance liquid chromatography (HPLC, Agilent, USA). In order to know the concentration of adsorbed TBBPA on Cu/Fe nanoparticles surface, TBBPA was extracted by methanol after adding concentrated HCl which was used to dissolve the adsorbed TBBPA on nanoparticles surface on a vortex orbital mixer (Genie 2, G560) and then analyzed by HPLC. The different extraction methods for adsorbed TBBPA were shown in Fig. S6. (Appendix).

3.5.3 Analytical methods of TBBPA

The TBBPA samples were placed into the autosampler vials and then analyzed by HPLC with a UV detector (Agilent) at 280 nm. A C18 column (Agilent, Eclipse XDB-C18, 250 mm × 4.6 mm) was used. The mobile phase of 80 % methanol (contained 1 % acetic acid) and 20 % Milli-Q water was delivered at a rate of 1 mL/min. Each sample size was 20 µL. The retention time of TBBPA in HPLC was about 6.2 min. Quantification was done with a calibration curve of the tetrabromobisphenol A standard.

29

3.5.4 Analysis of byproducts

The TBBPA byproducts, including tribromobisphenol A (tri-BBPA), dibromo-bisphenol A (di-BBPA), bromobisphenol A (mono-BBPA), and bisphenol A (BPA), which reacted with Cu/Fe bimetallic nanoparticles were monitored after the reactions. The concentrations of TBBPA were analyzed via the same HPLC with a UV detector at 280 nm and a C18 column. The mobile phase of 80 % methanol (contained 1 % acetic acid) and 20 % Milli-Q water was delivered at a rate of 0.8 mL/min. Each sample size was 20 μL. The column temperature was 30 ^{o}C. The retention times of TBBPA, tri-BBPA, di-BBPA and mono-BBPA on the chromatograms were 10.3, 6.7, 4.4, 3.3 min respectively. Because the mono-BBPA, di-BBPA and tri-BBPA were not commercially available, their concentrations in aqueous phase were determined from the chromatogram peak areas on a mass basis with compensation for the number of bromine based on the standard curves of TBBPA and BPA (Huang et al., 2013; Li et al., 2016).

The concentrations of BPA in the aqueous samples were also analyzed by same HPLC; and the same UV/Vis equipped with same column. The mobile phase was composed of 70 % methanol (contained 1 % acetic acid) and 30 % Milli-Q water at a flow rate of 0.8 mL/min. The sample loop was 20 μL. The retention time of BPA on the chromatograms was about 4.5 min. Quantification was done with a calibration curve of the bisphenol A standard.

These byproducts were collected with separated time and analyzed by high resolution negative-ion electrospray ionization mass spectrometry (HRESI(-)/MS) (Thermo Scientific, QE Plus, USA) in order to identified whether these byproducts were mono-BBPA, di-BBPA, and tri-BBPA.

3.5.5 Anion analysis

The bromide ions (Br^-) in solution produced during the debromination of TBBPA were quantified using an ion chromatography (IC, Methrohm, model 861 Advanced Compact IC, Switzerland) with an anion analytical column, Metrosep A sup 5-250/4.0. The mobile phase was anion eluent (composed of 3.2 mM Na_2CO_3 and $NaHCO_3$ 1.0 mM) at a flow rate of 0.7 mL/min. The sample size was 20µL and the concentration of standard bromide ions was sodium bromide solution. Suppressor was H_2SO_4 (about 0.5%). At the select time, the aqueous sample was withdrawn and diluted with ultrapure water for analysis. After diluting the sample five times, 3 mL sample was added to an autosampler tube and analyzed by IC.

3.5.6 Cation analysis

The concentration of dissolved ferrous ions was determined with a ferrozine method. To prepared ferroin indicator, 2.5 g of 1,10-phenanthroline hydrochloride was dissolved in 0.5 L Milli-Q water. Ammonium acetate solution for pH buffer was mixed 50 g ammonium acetate in 30 mL distilled water with 140 mL acetic acid. The reactions were carried out in a 4 mL volumetric bottle. 0.1 mL solution of the sample was mixed with 1 mL ferroin indicator, 0.5 mL ammonium acetate solution, 2.5 mL diluted hydrogen chloride aqueous solution, adjusted pH to weak acid by the buffer solution, and finally quantified by UV-Vis. UV-Vis spectrometer was used for estimating ferrous ion at 510 nm.

The concentration of Cu was measured by Cu probe and the instrument detection limit (IDL) was 0.001 mg/L.

3.5.7 TOC analysis
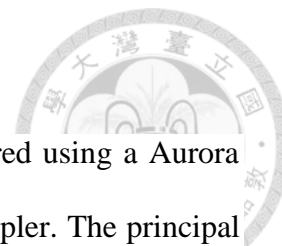
The concentration of total organic carbon (TOC) was measured using a Aurora Model 1030W TOC analyzer with an Aurora Model 1088 autosampler. The principal of the analyzer's operation is the use of sodium persulfate solution, UV radiation and temperature of 98 ℃ to oxidize organic carbon. During the analysis, samples are acidified by 17% phosphoric acid with 0.5 mL, sparged with nitrogen gas, and oxidized. Carbon dioxide formed in the oxidation process is subsequently quantified in an infrared detector (Stedmon et al., 2011). Potassium hydrogen phthalate served as a standard for comparison with sample results in each TOC run.

3.6 TBBPA removal modeling

3.6.1 TBBPA removal rate constants

The removal of TBBPA with Cu/Fe nanoparticles can be described as a pseudo-first-order reaction model.

$$dC/dt = -kC \qquad (3\text{-}4)$$

$$\ln (C_t/C_0) = -kt \qquad (3\text{-}5)$$

$$C_t = C_o e^{-kt} \qquad (3\text{-}6)$$

where C_t (mg/L) is the concentration of TBBPA at time t, C_0 (mg/L) is the initial concentration of TBBPA, $k(min^{-1})$ is the measured rate constants, and t is the reaction time (min).

3.6.2 Removal efficiency

Removal efficiencies of TBBPA reacted with Cu/Fe nanoparticles were calculated as the ratio of the concentration difference between the initial concentration of TBBPA and its final concentration to its initial concentration.
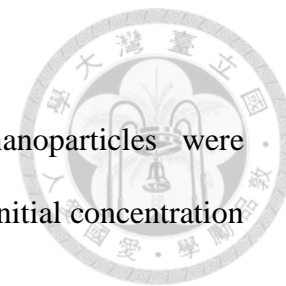
$$\text{Removal efficiency of TBBPA} = (C_0 - C_f)/C_0 \ (\%) \tag{3-7}$$

where C_f (mg/L) is the final concentration of TBBPA, and C_0 (mg/L) is the initial concentration of TBBPA.

3.6.3 Debromination efficiency

Debromination efficiency of TBBPA was calculated as the ratio of the measured concentration of bromide ions to the concentration of bromide ions theoretically produced by the complete debromination of TBBPA.

$$\text{Debromination efficiency} = (C_{Br^-})/(C_0 \times 4) \ (\%) \tag{3-8}$$

where C_{Br^-} (μM) is the molar concentration of Br^- production after reaction, and C_0 (μM) is the initial concentration of TBBPA.

3.6.4 Adsorption ratio and degradation ratio

To know the adsorption ratio of TBBPA on the Cu/Fe nanoparticle surface, HCl was used to dissolve the adsorbed TBBPA on nanoparticles surface and methanol acted as a solvent before analyzed by HPLC. The different extraction methods for

adsorbed TBBPA were shown in Fig. S6. (Appendix). The ratio of the adsorbed concentration of TBBPA to the initial concentration of TBBPA was defined as the adsorption ratio of TBBPA reacted with Cu/Fe nanoparticle. The difference between the removal efficiency of TBBPA and the adsorption ratio of TBBPA was defined as the degradation ratio of TBBPA.

$$\text{Adsorption ratio} = C_{ad}/C_0 \ (\%) \quad\quad\quad (3\text{-}9)$$

$$\text{Degradation ratio} = (\text{Removal efficiency of TBBPA}) - (\text{Adsorption ratio}) \quad (3\text{-}10)$$

where C_{ad} (mg/L) was the adsorbed concentration of TBBPA, and C_0 (mg/L) was the initial concentration of TBBPA.

34

Chapter 4 Results and Discussion

4.1 Characterization of Cu/Fe nanoparticles

The TEM and SEM images of synthesized Cu/Fe nanoparticles were presented in Figure 4-1. Figure 4-1a showed the synthesized nanoparticles which dispersed in the methanol appeared to be approximately spherical form with diameters less than 50 nm. It agreed with data reported in the literature of synthesized nanoparticles with diameters of 7-100 nm (Zhang and Manthiram, 1997; Zhuang et al, 2010). The surface area of synthesized Cu/Fe nanoparticles is 32.1 m^2/g. Figure 4-1b showed the synthesized nanoparticles formed chains of spheres in accordance with other iron-based nanoparticles in previous reports (Zhang and Manthiram, 1997; Schrick et al., 2002). Particle size distributions were calculated by Image J that have been reported in previous studies (Yang et al., 2013; Singh and Bose, 2015) and it was estimated from Figure 4-1a and shown in Figure 4-2, indicating that the mean particle size was 4.7 ± 3.7 nm.

Particle size distributions of nanoparticles suspended in solutions after synthesis and sonication were obtained by DLS (Figure 4-3). The particle sizes of synthesized bimetallic particles were measured by DLS with average diameter of 30 nm (Shih and Chen, 2010) and the mean particle size was around 36.7 ± 8.1 nm by DLS for synthesized Cu/Fe nanoparticles (Figure 4-3). Particle size calculated from TEM was much smaller than the mean particle size obtained by DLS. Due to the principle of DLS for size analysis, the particle value of size from DLS analysis is called "hydrodynamic diameter", which includes surrounding water molecules. Furthermore, nanoparticles are easily aggregated in water (Tso et al., 2010)

35
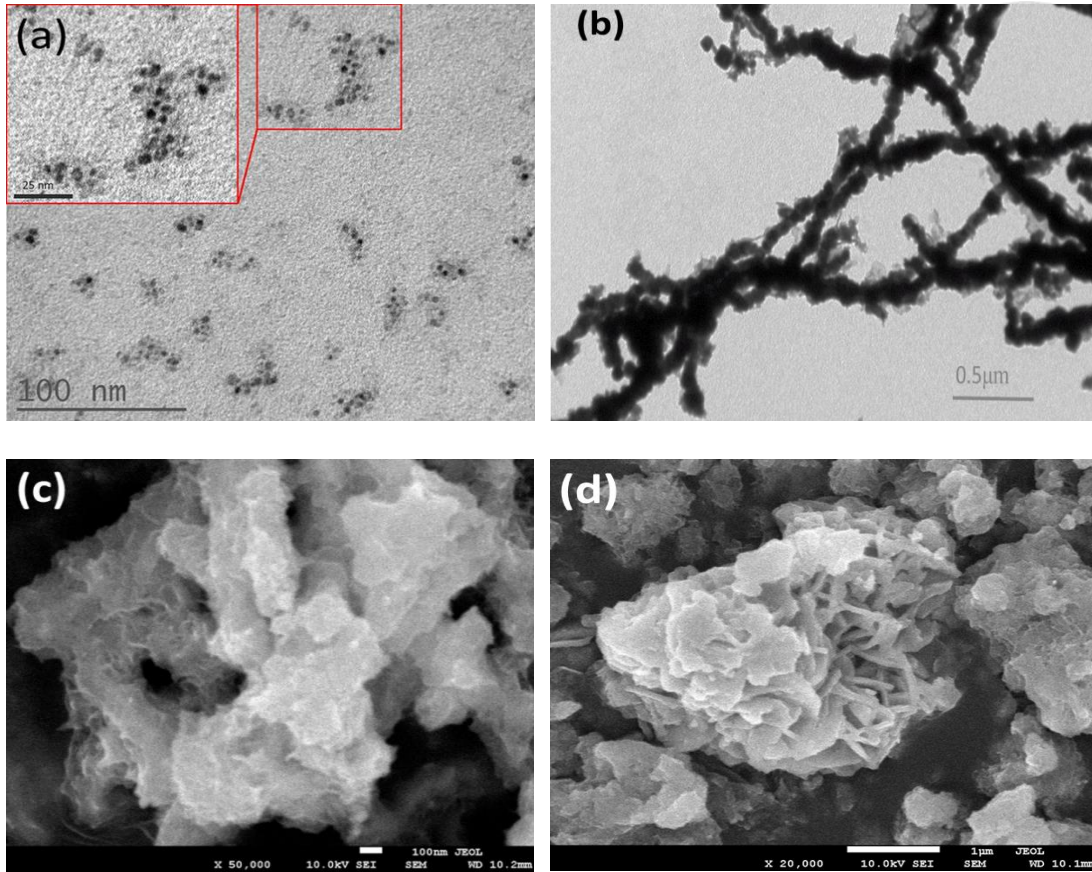
Figure 4-1 The electron microscopy images of Cu/Fe nanoparticles: (a) and (b) TEM, (c) and (d) SEM. (a) dispersion, (b) chain-liked aggregates, (c) and (d) aged nanoparticles (The Cu content of Cu/Fe nanoparticles is 4.0 %).
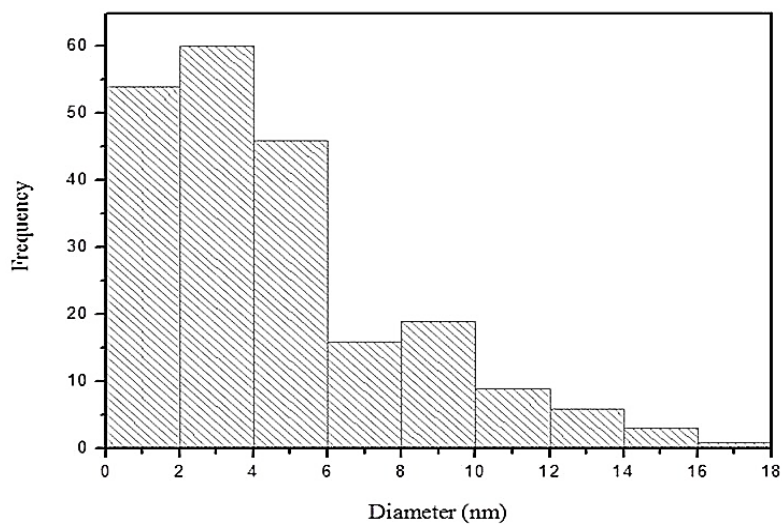
Figure 4-2 The particle size distributions for Cu/Fe nanoparticles calculated from Figure 4-1a.

36
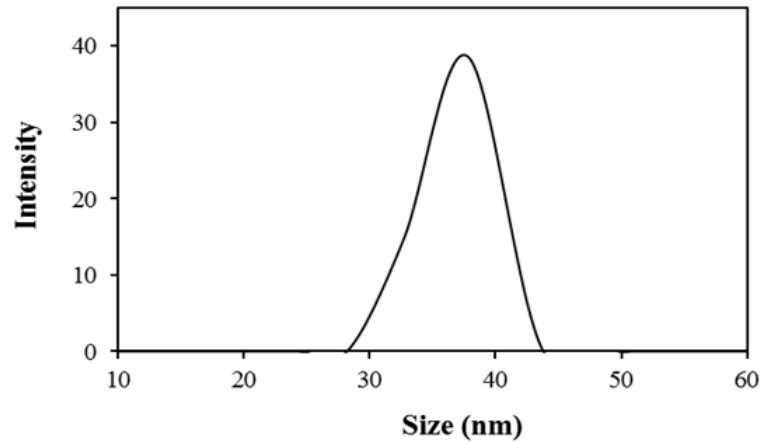
Figure 4-3 The particle size distributions for Cu/Fe nanoparticles by DLS.

The result of SEM-EDS analysis for elemental compositions of the synthesized bimetallic particles was shown in Figure 4-4. Several peaks for iron and copper were observed, indicated that copper successfully doped on the NZVI.
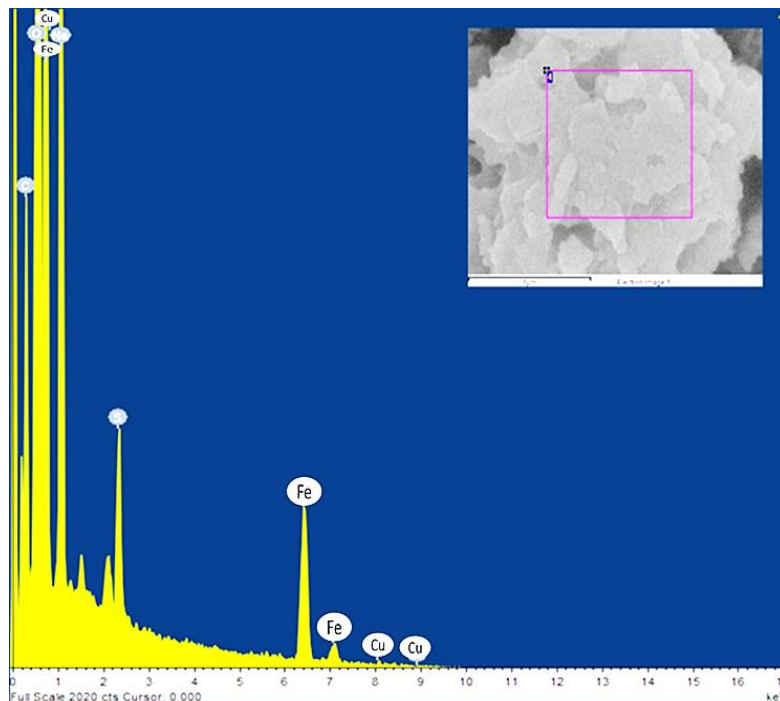
Figure 4-4 SEM energy-dispersive spectroscopy of Cu/Fe nanoparticles.

The XRD pattern of the synthesized Cu/Fe nanoparticles was shown in Figure 4-5. Zero valent states of iron and copper were observed at $2\theta = 44.1°$ and $43°$, respectively, which were also observed by Lai et al. (2014). However, the peak of iron oxide was observed at $2\theta = 62.7°$ with smaller intensity, which might be resulted from iron aged (Nurmi et al., 2005) or sample preparation. Actually, it was difficult to confirm the existence of zero valent copper on the NZVI from these weak peaks in this few amount of Cu because the main peaks of NZVI and zero valent copper were very close.
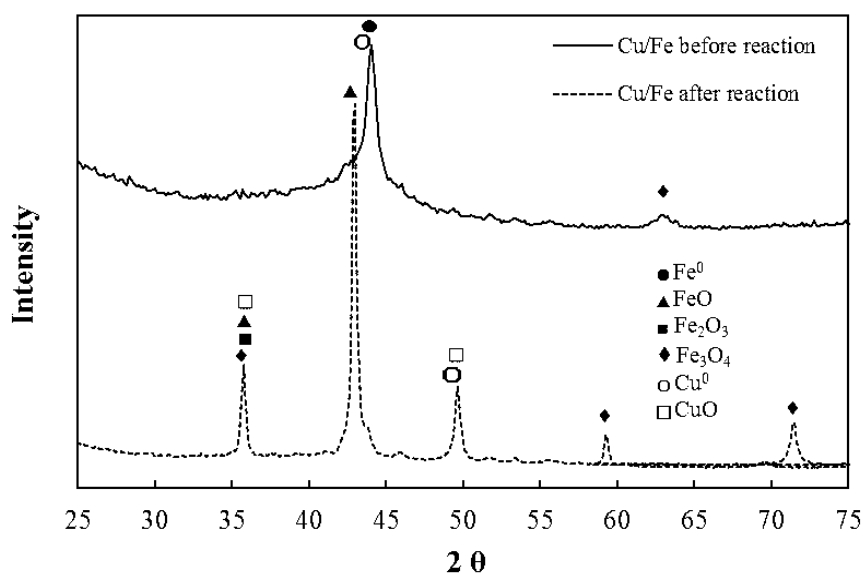
Figure 4-5 The XRD pattern of Cu/Fe bimetallic nanoparticles before and after reactions.

The normalized Fe and Cu K-edge XANES spectra of the synthesized Cu/Fe bimetallic nanoparticles were shown in Figure 4-6 and Figure 4-7, respectively. It was observed that Cu/Fe nanoparticles exhibited an obvious absorbance feature at 7112-7115 eV (Shih et al., 2016; Tso and Shih, 2016) for zero valent iron. Zero valent

copper would appear at 8979-8982 eV (Fulda et al, 2013). The linear combination fitting result of Fe K-edge XANES of Cu/Fe nanoparticles before reaction was shown in Table 4-1. The fitting results suggested the synthesized Cu/Fe NPs contain about 100 % zero valent iron and no iron oxides.
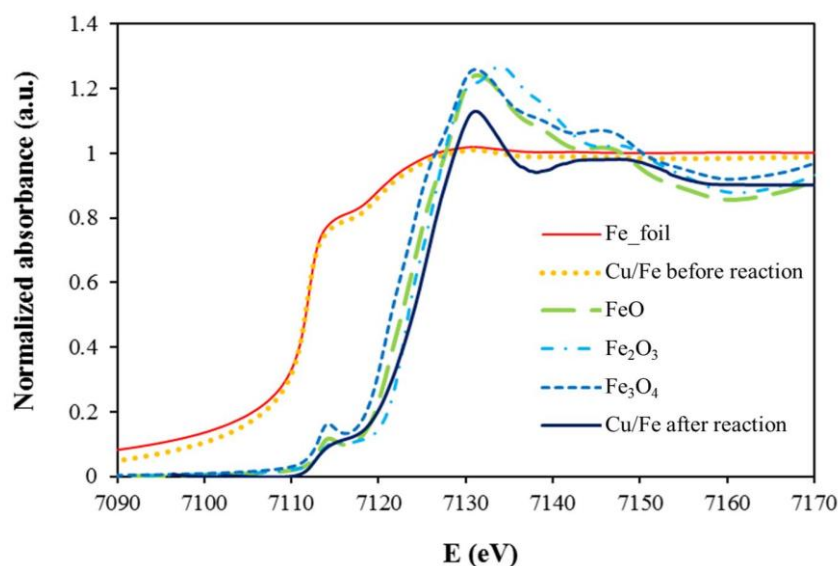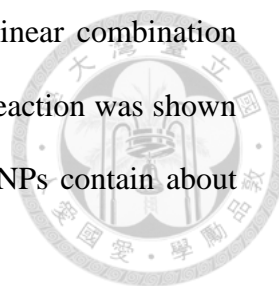
Figure 4-6 Fe K-edge XANES spectra of Cu/Fe nanoparticles before and after reaction.

Table 4-1 The linear combination fitting of Fe K-edge XANES spectra of Cu/Fe nanoparticles before and after reaction

Compound	Weight ratio (%)			
	Fe	FeO	Fe_2O_3	Fe_3O_4
Cu/Fe before reaction	100	0	0	0
Cu/Fe after reaction	65.2	34.8	0	0

Normalized Cu K-edge XANES was used to know whether the zero valent copper existed on the synthesized NZVI by determing the speciation of copper on the NZVI. In Figure 4-7, the absorbance features of Cu/Fe nanoparticles seem to like zero valent copper as similar as a previous study that was reported in Fulda et al. (2013).

39

The linear combination fitting of Cu K-edge XANES of Cu/Fe nanoparticles before reaction was shown in Table 4-2. The fitting results showed the detail of the synthesized Cu/Fe nanoparticles that contain about 68.4 % zero valent copper and 34.9 % CuO. The results indicated that during the preparation, copper ions could be reduced to zero valent copper by NZVI; however, zero valent copper might be oxidized to divalent copper during XANES the analysis.
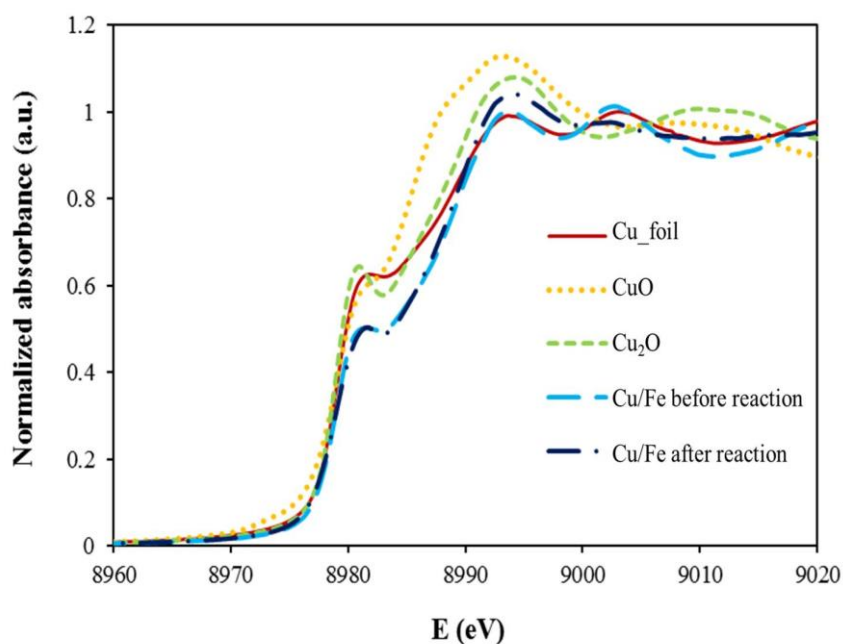
Figure 4-7 Cu K-edge XANES spectra of Cu/Fe nanoparticles before and after reaction.

Table 4-2 The linear combination fitting of Cu K-edge XANES spectra of Cu/Fe nanoparticles before and after reaction.

Compound	Weight ratio (%)		
	Cu	Cu_2O	CuO
Cu/Fe before reaction	68.4	0	34.9
Cu/Fe after reaction	23.3	54.7	22.1

Figure 4-8 showed the Raman spectra of synthesized Cu/Fe nanoparticles to study whether the metallic oxides appear on the Cu/Fe nanoparticles. At various pH conditions (pH 7 and 11), there were no obvious metallic oxides on the freshly synthesized Cu/Fe nanoparticles.
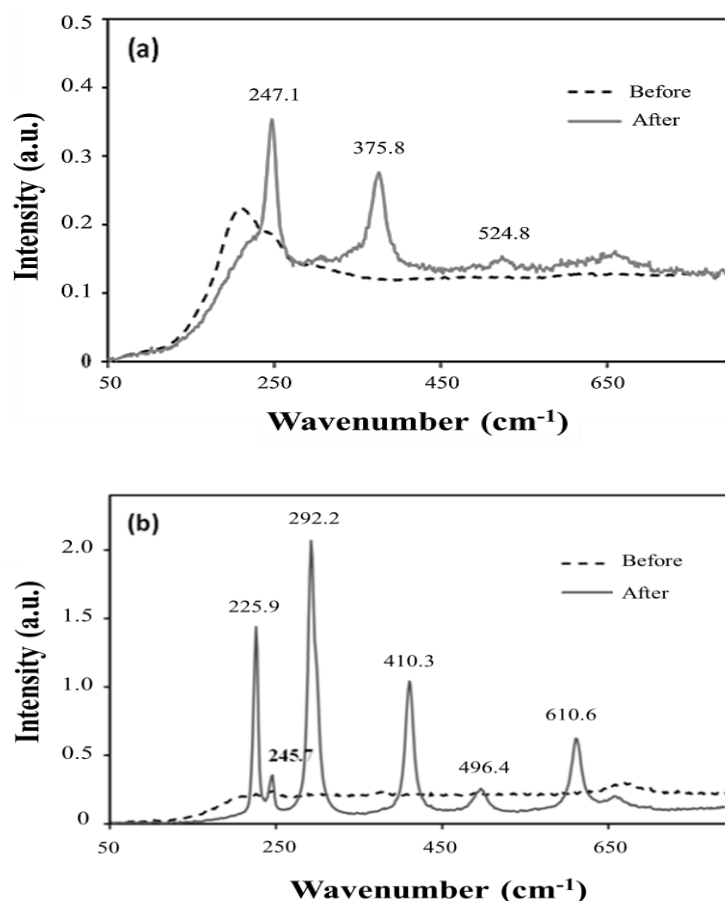
Figure 4-8 Raman spectra of Cu/Fe nanoparticles at (a) pH 7.0 and (b) pH 11.0.

4.2 Effect of copper content on the removal of TBBPA by Cu/Fe nanoparticles

In order to investigate the effect of nickle and copper contents in Cu/Fe nanoparticles and to find an optimal percentage of copper loading in Cu/Fe bimetallic nanoparticle systems on the removal of TBBPA in solutions, four batches of

41

experiments were performed. The dosage of Ni/Fe and Cu/Fe nanoparticles was 2.0 g/L and the initial concentration of TBBPA was 5.0 mg/L. The copper ratio of Ni/Fe and Cu/Fe bimetallic nanoparticles ranged from 0.5 % to 8 %.

As shown in Figure 4-9, when the content of copper increased between 0.5 % and 4 %, the concentration of TBBPA rapidly decreased. It was also observed in Ni/Fe nanoparticles (Table S1). Nevertheless, when the content of copper increased up to 8 %, the removal kinetics of TBBPA decrease slightly as shown in Table 4-3. The removal rate constants of TBBPA increased as the Cu loading was increased from 0.5, 2.0 to 4.0 wt.% and dropped when the Cu loading was 8.0 wt.%. The rate constants were determined as 0.145, 0.173, 0.229 and 0.160 min^{-1} for 0.5, 2.0, 4.0 and 8.0 wt. %, respectively. The most suitable copper percentage was 4.0 %. Ion-based bimetallic particles could be used to treat organic compounds effectively. For bimetallic iron, galvanic couples formed between the iron and the second metal that could improve the electron transfer from NZVI to organic compounds (Tian et al., 2009). The result was also consistent with Yuan et al. (2014), reported that the removal rate constants of one dye (acid orange 7) increased from 0.069 to 0.108 min^{-1} with the increment of Cu mass loading from 0.11 to 0.62 g of Cu/g of Fe. Subsequently, the continuous increase of Cu mass loading could result in a decrease of the rate constants. It was resulted from that the number of formed galvanic couples gradually decreased as the proportion of Fe^0 in Cu/Fe bimetallic particles decreased. Tee et al. (2005) conducted the TCE dechlorination studies with Ni/Fe nanoparticles. It concluded that the formation of a less-reactive nickel-rich surface layer on the nanoparticles in a very high nickel content in the Ni/Fe nanoparticles made a detrimental effect on the degradation reaction.
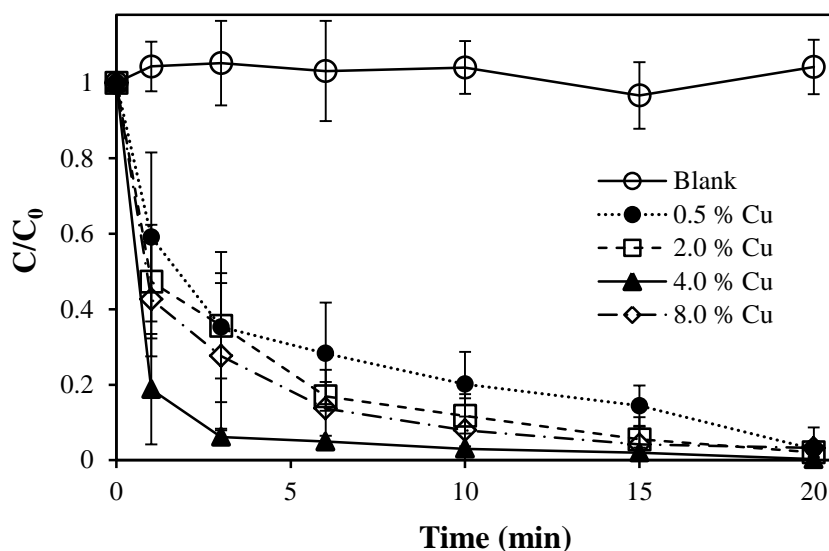
Figure 4-9 Effect of Cu content on the removal of TBBPA by Cu/Fe nanoparticles (The reaction solutions contained 2.0 g/L of Cu/Fe particles and 5.0 mg/L of TBBPA).

Table 4-3 The removal rate constants and removal efficiencies of TBBPA by Cu/Fe nanoparticles at various percentages of copper.

Cu content (%)	k (min^{-1})	Removal efficiency (%)	Br- concentration (μM)	Debromination efficiency (%)
0.5	0.145	97.1 ± 2.0	22.4 ± 4.3	60.8 ± 11.7
2	0.173	97.9 ± 3.0	29.2 ± 6.9	79.3 ± 18.8
4	0.229	99.8 ± 0.3	34.8 ± 2.2	94.7 ± 6.0
8	0.160	96.8 ± 5.5	26.9 ± 2.5	73.2 ± 4.1

The method detection limit (MDL) of TBBPA is 0.1 mg/L.

The removal efficiencies of TBBPA were 97.1 %, 97.9 %, 99.8 % and 96.8% for 0.5, 2.0, 4.0, and 8.0 wt. % Cu, respectively. The results indicated that while the copper content increases, the removal efficiencies of TBBPA could gradually increase first and decrease later. In 20 minutes, all treatments show the high removal efficiencies of TBBPA in aqueous solution. Feng and Lim (2005) published that more active site could

43

be generated on the iron surface with Ni content increasing. However, at a high Ni content, it could not deposit in mono-dispersion on the iron surface. Fine particles or discrete deposits could form in the reaction solutions, and some of the active site would be covered that resulted in the drop of rate constant and removal efficiency when the second metal at a high content (Yuan et al., 2014; Zhuang et al., 2012; Feng and Lim, 2005).

In addition, the debromination efficiencies of TBBPA increased from 60.8 %, 79.3 % to 94.7 % and then decreased to 73.2 % for copper content of 0.5 %, 2.0 %, 4.0 % and 8.0 % after 20 min of reaction as shown in Table 4-3.

For bimetallic iron, galvanic couples formed between the iron and the second metal, while iron acted as the anode and the second metal acted as the cathode, and the electron were induced to flow from iron to the second metal (Cwiertny et al., 2007) that could promote dechlorination (Elliott and Zhang, 2001). Luo et al. (2010) reported that the debromination rate constant of TBBPA increased with the Ag coverage rising. Zhuang et al. (2011) also showed the debromination reaction rate of PBDEs can be significantly increased by coating of Pd on the NZVI. The second metals on the nanoscale Fe particles surface serves as a collector of hydrogen gas that resulted from the corrosion of Fe (Fang et al., 2011), and the atomic hydrogen adsorbed on the second metal surface (Cwiertny et al., 2007; Wang et al., 2009) that could facilitate dehalogenation (Fang et al., 2011). Huang et al. (2015) also indicated that the debromination rate of TBBPA was closely related to the total Pd site on ZVI surface.

Figure 4-10 showed the concentration of bromide ion (Br$^-$) and TBBPA debrominated byproduct, bisphenol A (BPA). These results were consistent with the TBBPA removal kinetics and TBBPA debromination mentioned above. With copper content increased between the 0.5 % and 4 % of copper content, the concentration of

Br⁻ increased and accompanied with the increased concentration of BPA.
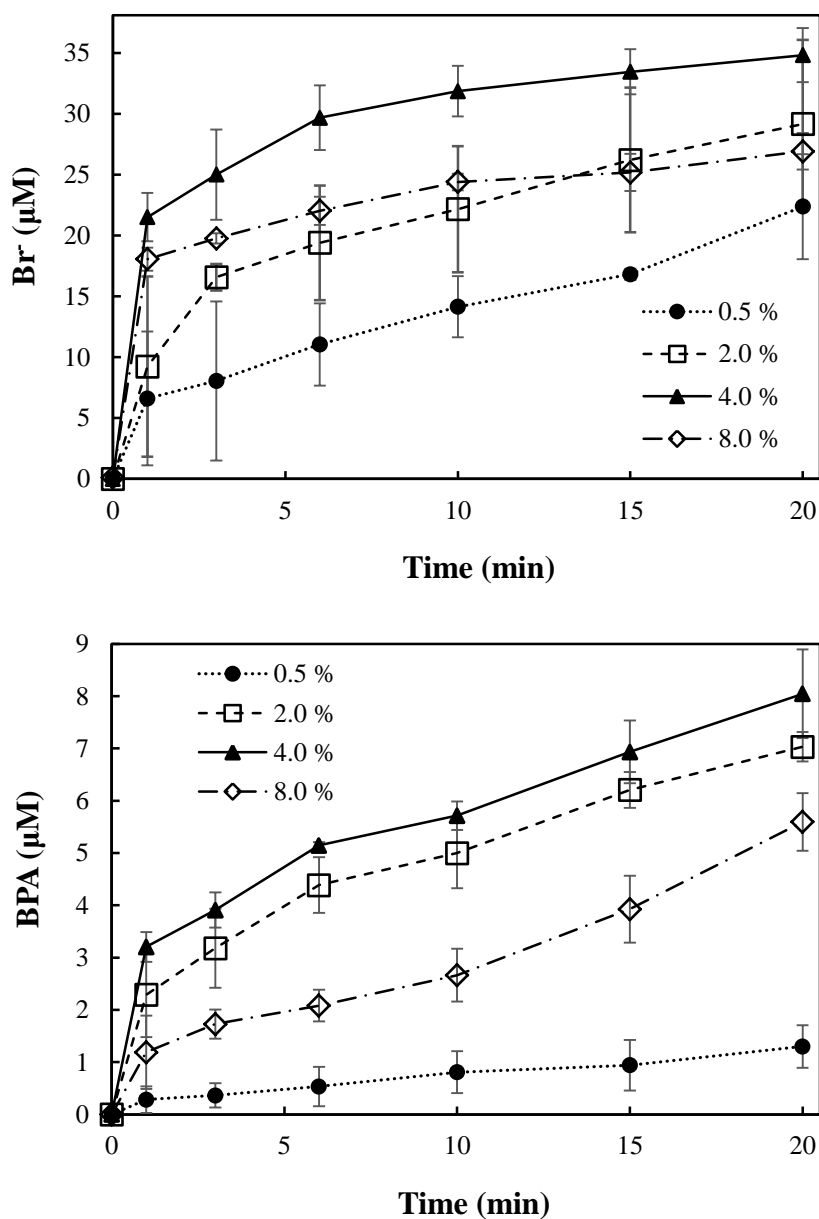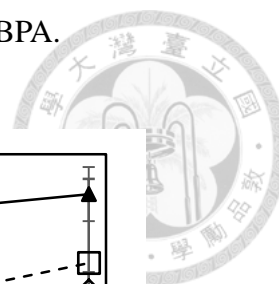
Figure 4-10 The concentration of (a) Br⁻ and (b) BPA with TBBPA removed by Cu/Fe nanoparticles with different Cu content. (The reaction solutions initially contained 2.0 g/L of Cu/Fe particles and 5.0 mg/L of TBBPA).

The kinetics of TBBPA removal by NZVI and Ni/Fe nanoparticle with various Ni content were shown in Figure S2 and Figure S3. Comparing NZVI, Ni/Fe and Cu/Fe nanoparticles, 4 % Cu in Cu/Fe nanoparticles has the highest removal rate (Table S1

45

and Table 4-3). In the same percentage of Ni and Cu in bimetallic, Cu/Fe has a higher removal rate and removal efficiency.

4.3 Effect of dosage of Cu/Fe on the removal of TBBPA by Cu/Fe nanoparticles

Four batches of experiments were performed to evaluate the effect of various Cu/Fe dosages on the removal of TBBPA by Cu/Fe nanoparticles in the aqueous solutions (Figure 4-11). The percentage of Cu content on iron was 4 % and the initial concentration of TBBPA was 5.0 mg/L. The dosages of Cu/Fe nanoparticles were 1.0, 2.0, 3.0, and 4.0 g/L.

As shown in Figure 4-11, the concentration of TBBPA dramatically dropped with time when the Cu/Fe nanoparticles were added in the solution. In 20 minutes, almost 100 % TBBPA was removed in different reaction solution with various nanoparticles dosage. However, it had obvious difference in 1 min, the remaining TBBPA percentages were 49.2, 18.8, 7.0, and 4.2 % for 1.0, 2.0, 3.0, and 4.0 g/L, respectively. Furthermore, the removal rate constants of TBBPA with 1.0, 2.0, 3.0, and 4.0 g/L Cu/Fe nanoparticles were estimated to be 0.216, 0.229, 0.347, and 0.387 min^{-1}, respectively (Table 4-4). Increasing the dosage of Cu/Fe nanoparticles in the removal reactions can enhance the removal rates of TBBPA. The removal rate constant and removal efficiency of organic compounds have a strong dependence on the dosage of bimetallic particles and the reaction occurred at the Fe-M-H_2O (M = second metals) interface (Bokare et al., 2008) that was a surface-mediated process (Li et al., 2016). Fang et al. (2011) studied the degradation BDE209 with nanoparticles and reported that the number of active sites and reactive surface areas could increase simultaneously when the increment of Ni/Fe particle. The loading of bimetallic

46

nanoparticles increased the degradation rate constant (Bokare et al., 2008; Huang et al., 2015). The removal rate constant for TBBPA removal by Cu/Fe nanoparticles herein were higher than TBBPA removal with the Ni/Fe nanoparticles reported by Li et al. (2016). The lower removal rate constant by Ni/Fe was attributed to the effect of cosolvent, methanol for available hydrogen (Lin et al., 2012).
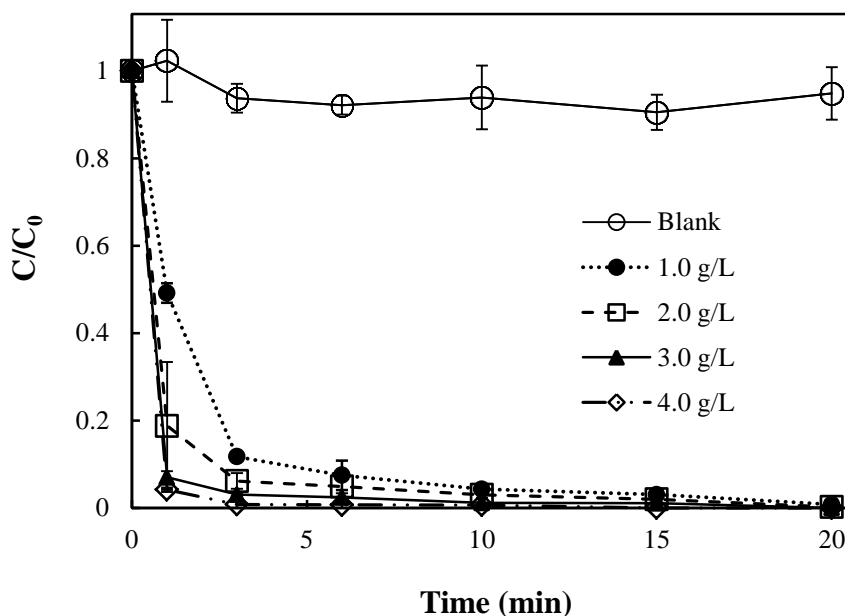
Figure 4-11 Effect of Cu/Fe nanoparticle dosages on the removal of TBBPA by Cu/Fe nanoparticles ([TBBPA] = 5 mg/L and Cu content was 4.0 %).

As the Cu/Fe dosage gradually increased from 1.0, 2.0, 3.0 to 4.0 g/L, the removal efficiencies of TBBPA were 99.2%, 99.8%, 100%, and 100%, respectively (Table 4-4). The results showed that the dosage has no significant effects on the removal efficiencies after 20 minutes, and all treatments show the high removal efficiencies of TBBPA in aqueous solution. Besides, it also meant that a low dosage of bimetallic nanoparticles, 1.0 g/L, had the ability to remove a high concentration of TBBPA with 5.0 mg/L in a longer time of 30 minutes.

The debromination efficiencies of TBBPA were higher than 89% (Table 4-4).

47

Moreover, the debromination efficiencies were raised from 88.7 %, 94.7 %, 95.2 % to 105.9 % for the increased dosage of Cu/Fe nanoparticles with 1.0, 2.0, 3.0, and 4.0 g/L (Table 4-4). As more nanoparticles were added in the reaction solution, the more bromide ions were released from TBBPA (Figure 4-17a) and no bromide ion exist in control that without any nanoparticles.

Table 4-4 The removal rate constants and removal efficiencies of TBBPA by Cu/Fe nanoparticles at various Cu/Fe dosages.

Cu/Fe dosage (g/L)	k (min^{-1})	Removal efficiency (%)	Br$^-$ concentration (μM)	Debromination efficiency (%)
1.0	0.216	99.2 ± 1.1	32.6 ± 2.2	88.7 ± 6.1
2.0	0.229	99.8 ± 0.3	34.8 ± 2.2	94.7 ± 6.0
3.0	0.347	100.0 ± 0.0	35.0 ± 3.2	95.2 ± 8.7
4.0	0.387	100.0 ± 0.0	38.9 ± 5.1	105.5 ± 14.0

The MDL of TBBPA is 0.1 mg/L.

Additionally, with the TBBPA being debrominated, the concentrations of BPA dramatically increased (Figure 4-12b). Increasing the dosage of nanoparticles could enhance the debromination efficiency (Table 4-4) and increase the concentration of brominated byproducts (Figure 4-12b). It was in accordance with one report that a high dose of NZVI can enhance the debromination rate of HCB (Shih et al., 2011), due to more surface sites for reaction with HCB.
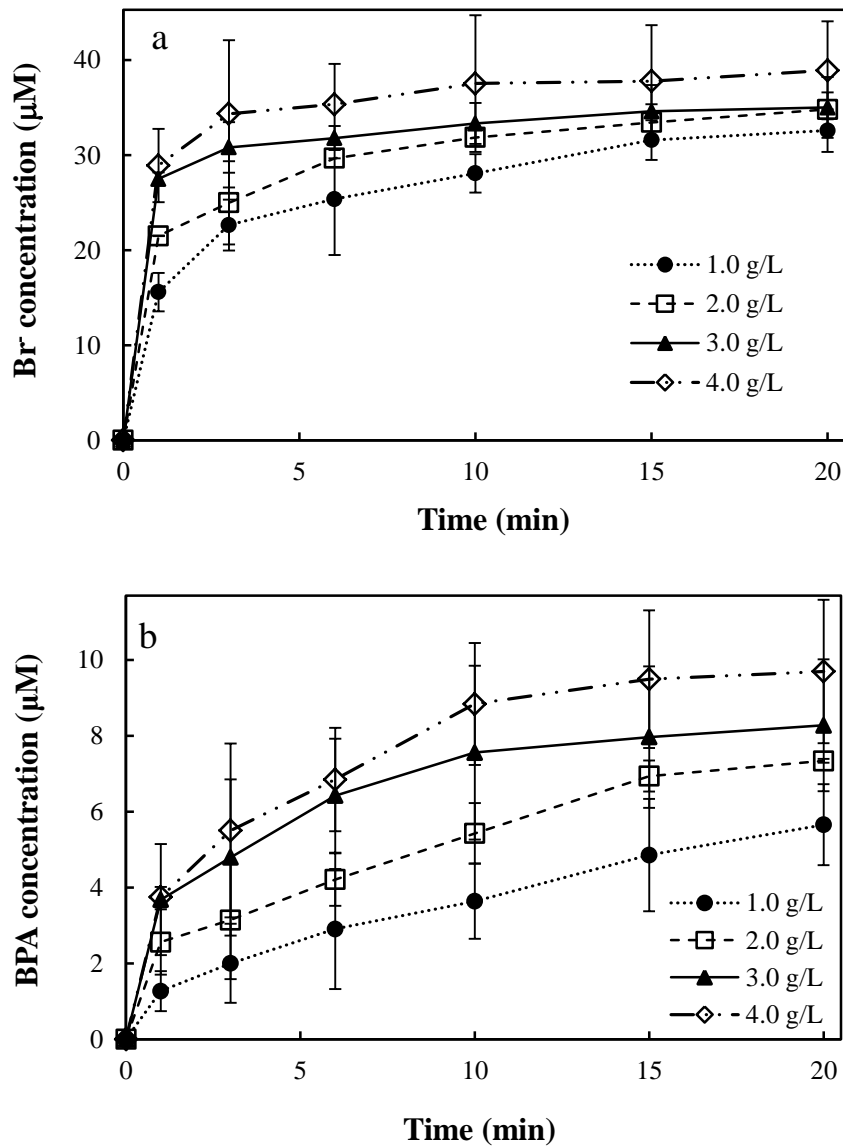
Figure 4-12 The concentration of (a) Br⁻ and (b) BPA generated from TBBPA by Cu/Fe nanoparticles as a function of the Cu/Fe dosage (The concentration of TBBPA is 5 mg/L and Cu content is 4 %).

4.4 Effect of initial TBBPA concentration on its removal by Cu/Fe nanoparticles

The effect of initial TBBPA concentration on the removal of TBBPA by Cu/Fe nanoparticles was investigated with four batch experiments. The dosage of Cu/Fe nanoparticles was 2.0 g/L and the percentage of copper was 4%. The initial

49

concentrations of TBBPA were conducted in this study for 1.0 mg/L, 5.0 mg/L, 10.0 mg/L and 15.0 mg/L.

Figure 4-13 showed the effect of the initial concentrations of TBBPA on the removal of TBBPA by Cu/Fe nanoparticles. In 20 minutes, 2.0 g/L of synthesized Cu/Fe nanoparticles removed over 50 % of TBBPA with various initial concentrations of TBBPA. The removal rate constant increased with the decreasing initial concentrations of TBBPA (Table 4-5).

Figure 4-13 Effect of initial concentration of TBBPA on the removal of TBBPA by Cu/Fe nanoparticles (The dosage of Cu/Fe nanoparticles was 2.0 g/L).

Table 4-5 shows the removal rate of TBBPA under initial TBBPA concentrations of 1 mg/L, 5 mg/L, 10 mg/L, and 15 mg/L were 0.392, 0.229, 0.217, and 0.178 min^{-1}, respectively. After the reaction with 20 min, the removal efficiencies were approaching to 100 % (Table 4-5). The removal efficiencies were 100 %, 99.8 %, 99.3 %, and 97.9 % for the TBBPA concentrations of 1 mg/L, 5 mg/L, 10 mg/L, and 15 mg/L, respectively (Table 4-5). Lin et al. (2012) reported that the reaction rate constant decreased as the initial concentration of TBBPA increased when reacting

50

with NZVI. Furthermore, Li et al. (2016) also gave the same conclusion that the removal rate constant rose as TBBPA at a lower concentration reacted with the same dosage of Ni/Fe nanoparticles ([Ni/Fe] = 2.0 g/L). The removal rate constant decreased from 0.054 min^{-1} to 0.018 min^{-1} for the initial TBBPA concentration between 5 mg/L and 15 mg/L. It was comparable with our results that of Cu/Fe nanoparticles with fewer methanol that was acted as a cosolvent and that could affect TBBPA removal by Cu/Fe nanoparticles (Figure S5).

Table 4-5 The removal rate constants, removal efficiencies and debromination efficiencies of TBBPA by Cu/Fe nanoparticles at various initial TBBPA concentration

TBBPA con. (mg/L)	k (min^{-1})	Removal efficiency (%)	Br^- concentration (μM)	Debromination efficiency (%)
1.0	0.392	100.0 ± 0.0	8.1 ± 0.8	110.4 ± 10.9
5.0	0.229	99.8 ± 0.3	34.8 ± 2.2	94.7 ± 6.0
10.0	0.217	99.3 ± 0.3	69.3 ± 2.8	94.2 ± 1.4
15.0	0.178	97.9 ± 1.0	104.4 ± 2.5	94.6 ± 2.6

The MDL of TBBPA is 0.1 mg/L.

Yuan et al. (2014) suggest that the degradation of Acid Orange 7 (AO7) in Cu/Fe bimetallic particles involves adsorption of AO7 on the reactive sites of Cu/Fe bimetallic particles, degradation reaction, and release of the degradation products. For halogenated organic compound, the degradation of BDE209 in the Ni/Fe nanoparticles system was also a heterogeneous reaction, which involves adsorption of the BDE209 on the Ni surface and the subsequent surface reaction (Fang et al., 2011). A high initial concentration of organic compounds would lead to competitive adsorption between the organic compounds molecules when the number of bimetallic

51

particles reactive site was fixed (Lin et al., 2012). This would decrease the number of organic compounds molecules adsorbed and reduced on the bimetallic particles, leading to a decrease in the degradation efficiency (Fang et al., 2011).

However, the removal amount increased from 0.50 to 7.34 mg/L in 20 min as the initial concentration of TBBPA increased from 1.0 mg/L to 15 mg/L (Figure 4-14). Comparing with the removal amount by Li et al. (2016), there was no difference with 5.0 mg/L and 10.0 mg/L of TBBPA, but Cu/Fe nanoparticles have a higher removal amount than Ni/Fe nanoparticles with 15.0 mg/L of TBBPA.

The debromination efficiencies in the sequence from 1.0 mg/L to 15.0 mg/L were 110.4 %, 94.7 %, 94.2 %, and 94.6 % (Table 4-5). The reactive sites of nanoparticles could be completed by TBBPA at a high concentration of TBBPA and made the debromination decline (Li et al. 2016; Lin et al, 2012). However, it indicated that the synthesized Cu/Fe bimetallic nanoparticles have a high ability to debrominate high concentration of TBBPA with 2.0 g/L of Cu/Fe.
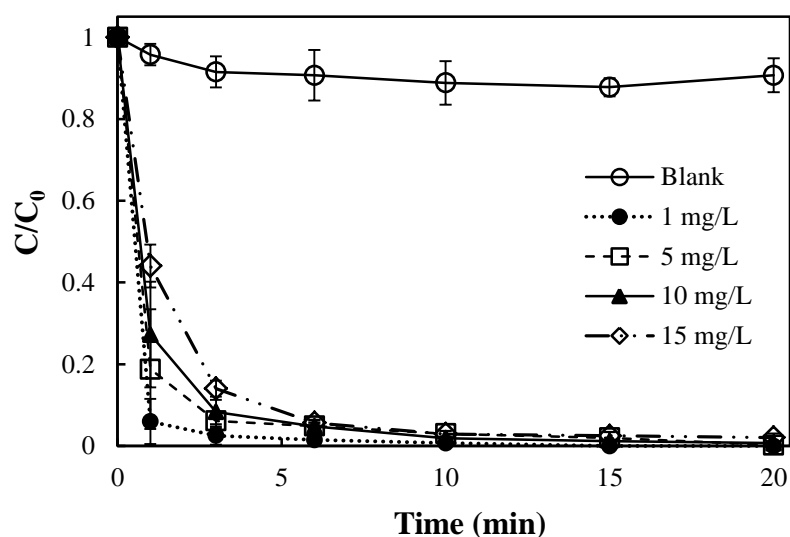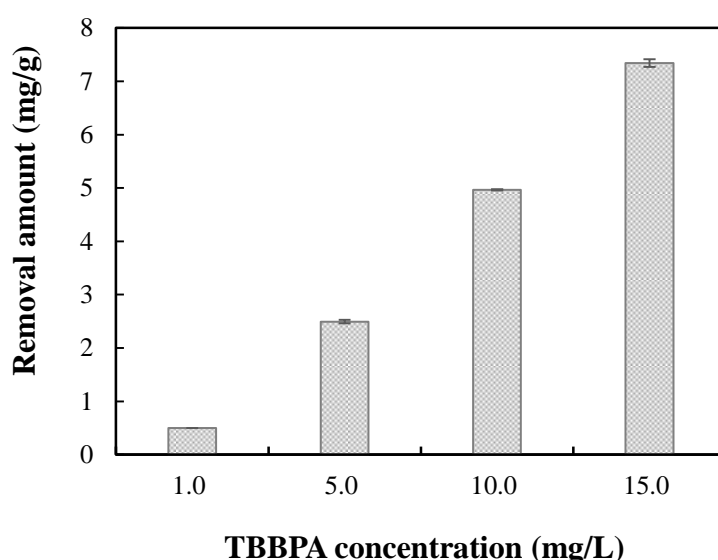

Figure 4-14 Effect of initial concentration of TBBPA on the removal amount in mg (TBBPA)/ g (Cu/Fe nanoparticles) (The dosage of Cu/Fe nanoparticles was 2.0 g/L).

4.5 Effect of temperature on the removal of TBBPA by Cu/Fe nanoparticles

The effect of temperature on the removal of TBBPA by Cu/Fe nanoparticles was performed at 5 $^{\circ}$C, 15 $^{\circ}$C, 25 $^{\circ}$C, 35 $^{\circ}$C, and 45 $^{\circ}$C, respectively (Figure 4-23). The dosage of Cu/Fe nanoparticles was 2.0 g/L and the percentage of copper was 4%. The initial concentrations of TBBPA was 5.0 mg/L.
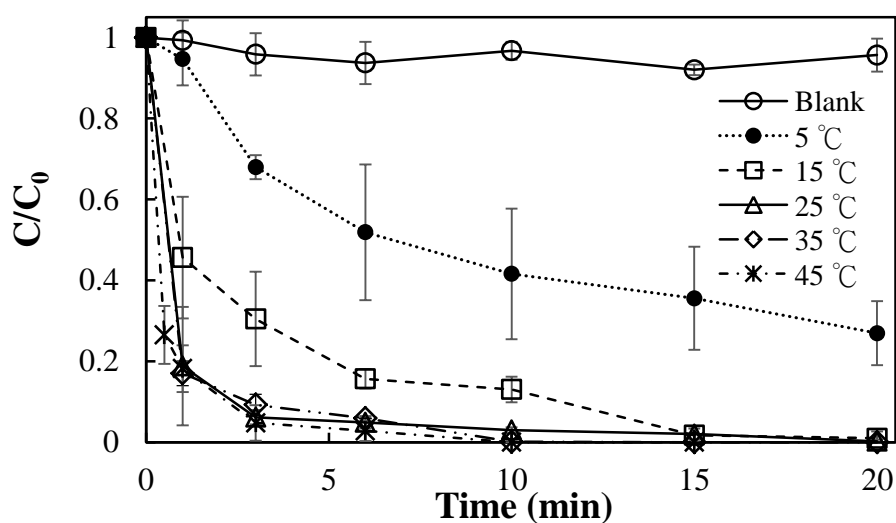
Figure 4-15 Effect of temperature on the removal of TBBPA by Cu/Fe nanoparticles ([Cu/Fe] = 2.0 g/L and [TBBPA] = 5.0 mg/L).

As shown in Figure 4-15 and Table 4-6, the removal efficiencies were 73.1 %, 99.0 %, 99.8 %, 100 %, and 100 % for 5 $^{\circ}$C, 15 $^{\circ}$C, 25 $^{\circ}$C, 35 $^{\circ}$C, and 45 $^{\circ}$C, respectively. The removal rate constants of TBBPA with Cu/Fe nanoparticles at 5 $^{\circ}$C, 15 $^{\circ}$C, 25 $^{\circ}$C, 35 $^{\circ}$C, and 45 $^{\circ}$C were estimated to be 0.064, 0.221, 0.229, 0.401, and 0.525 min^{-1}, respectively. The results indicated that TBBPA removal efficiency and rate constant increased with increasing temperature in the reaction. A similar result was also observed by Tso and Shih (2014) that as the temperature increases, the removal kinetics of HBCD by NZVI aggregates increases.

53

Table 4-6 The removal rate constants, removal efficiencies and debromination efficiencies of TBBPA by Cu/Fe nanoparticles at various temperature

Temperature (℃)	k (min^{-1})	Removal efficiency (%)	Br$^-$ concentration (μM)	Debromination efficiency (%)
5	0.064	73.1 ± 7.9	12.9	35.1
15	0.221	99.0 ± 1.7	24.5	66.7
25	0.229	99.8 ± 0.3	34.8	94.7
35	0.401	100.0 ± 0.0	35.2	95.6
45	0.525	100.0 ± 0.0	36.1	98.2

The MDL of TBBPA is 0.1 mg/L.

Figure 4-16 shows a plot of natural logarithm of rate constants for TBBPA removal versus 1/T. The slop of the plots was assigned as a ratio of activation energy to the ideal gas constant 8.314 kJ mol^{-1} K^{-1}. The activation energies of TBBPA removal by Cu/Fe nanoparticles was 35.64 kJ/mol. The surface-controlled reactions have larger activation energies (>29 kJ/mol) (Brezonik, 1994; Lien and Zhang, 2007). It suggested that the removal of TBBPA by Cu/Fe nanoparticles is a surface-control process.

y = -4.2872x + 12.954
R² = 0.8954
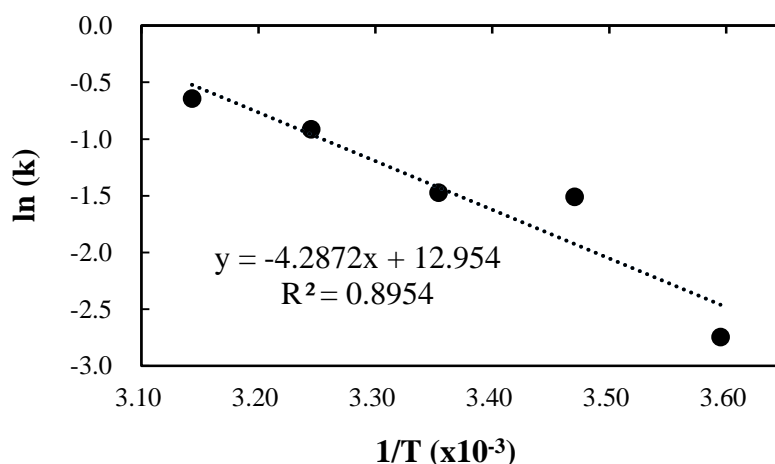
Figure 4-16 The plot of ln (k) versus 1/T: for TBBPA removal by Cu/Fe nanoparticles.

54

The debromination efficiencies of TBBPA were 35.1 %, 66.7 %, 94.7%, 95.6, and 98.2 % for 5 $^{\circ}$C, 15 $^{\circ}$C, 25 $^{\circ}$C, 35 $^{\circ}$C, and 45 $^{\circ}$C, respectively (Figure 4-17 and Table 4-6). Shih et al. (2011) suggested that temperature can facilitate the degradation of HCB by NZVI in aqueous solution through a stepwise reductive dechloronation mechanism.
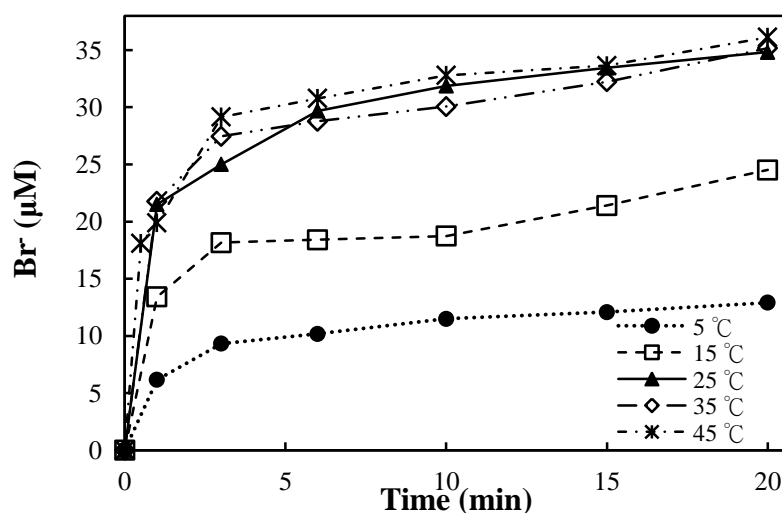
Figure 4-17 The concentration of Br$^-$ generated from TBBPA by Cu/Fe nanoparticles with various temperature ([TBBPA] = 5.0 mg/L and Cu content is 4.0 %).

4.6 Effect of initial pH on the removal of TBBPA by Cu/Fe nanoparticles

Five batch experiments were assessed to understand the effect of initial pH value in reaction solution on the removal of TBBPA by Cu/Fe nanoparticles (Figure 4-18). The dosage of Cu/Fe nanoparticle was 2.0 g/L, the percentage of copper was 4.0 % and the initial concentration of TBBPA was 5.0 mg/L. The different initial pH value of five reaction solutions was adjusted to 3.0, 5.0, 7.0, 9.0, and 11.0, respectively.

As shown in Figure 4-18, under an acid condition to slight alkaline one (pH 3.0-9.0), the TBBPA concentration drop dramatically; however, under alkaline

55

condition (pH 11.0), the TBBPA concentration decreased slowly.
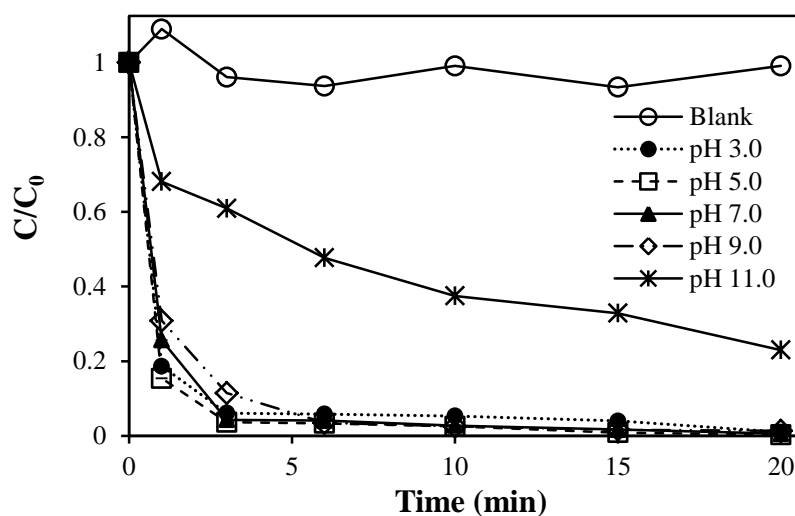
Figure 4-18 Effect of initial pH on the removal of TBBPA by Cu/Fe particles. The reaction solutions initially contained 2.0 g/L of Cu/Fe particles and 5.0 mg/L of TBBPA.

After adding the Cu/Fe nanoparticles, the pH of reaction solution was close to pH 8 for the initial pH range from 3.0 to 9.0 (Table 4-7). At an alkaline condition, ferrous hydroxide or iron oxides might be produced and occupy the reactive sites (Zhang, 2003) that resulted in lowering the electron transfer and reducing power (Chatterjee et al., 2010; Li et al., 2016), and caused the decrease of debromination efficiency that made the concentration of halogenated organic contaminants drop slowly.

Fang and Al-Abed (2008) reported that the conversion value of 2-chlorobiphenyl by Pd/Fe bimetallic particles decreased with increasing pH in solutions with a pH lower than 12.5. Huang et al. (2013) studied that the rate constants of TBBPA transformation with Pd/Fe nanoparticles decreased with pH increasing, and the best fit k values for the disappearance of TBBPA were 260 ± 3, 140 ± 9, 56 ± 5 and $7.7 \pm 0.5 \times 10^{-2}$ min^{-1} for the solution pH 4.2, 5.2, 6.2, and 7.2, respectively.
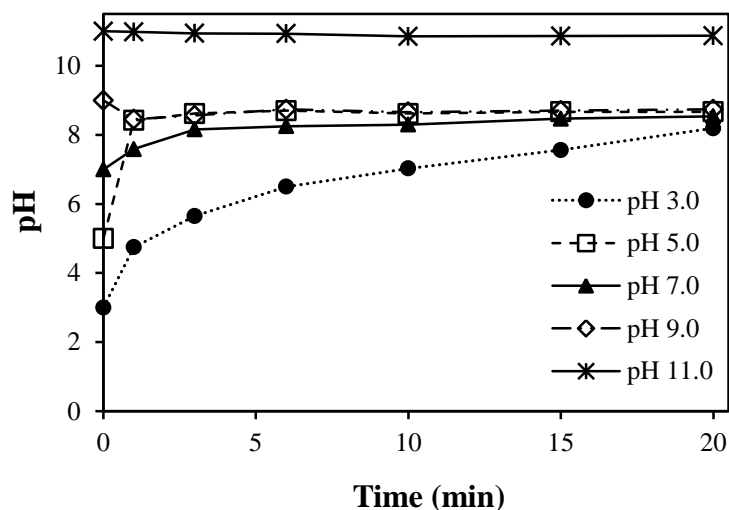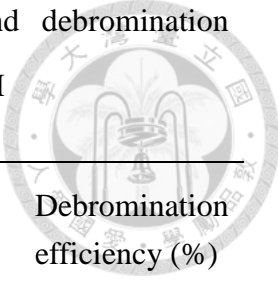
Figure 4-19 The pH change with time during the reactions at different initial pHs.

The rate constant varied with the solution pH, with the pH increasing between pH 5.0 to pH 11.0, the removal rate decreased (Table 4-7). The rate constants were 0.162, 0.228, 0.204, 0.191, and 0.063 min^{-1} for pH 3.0, 5.0, 7.0, 9.0, and 11.0, respectively (Table 4-7). Compared to pH 5.0, the removal rate constant was slower and the removal efficiency slight decreased at pH 3.0 that might cause by some of the Cu/Fe nanoparticles dissolved. Yuan et al. (2014) reported that under acidic conditions, ZVI will be quickly corroded and consumed that would seriously reduce the operational life span of ZVI. Besides, some researches indicated that small H_2 bubbles that produced from rapid corrosion of iron at the surface might act as a barrier (Matheson and Tratnyek, 1994; Graham and Jovanovic, 1999; Wang et al., 2009).

Table 4-7 demonstrated the effect of solution pH on the TBBPA removal efficiency, the removal efficiency was extremely high from pH 3.0 to pH 9.0, with over 98 % TBBPA removed within 20 min. However, the removal efficiency dramatically decreased at an alkaline solution. The final removal efficiencies from pH 3.0 to pH 11.0 were 99.0 %, 99.7 %, 99.4 %, 98.7 %, and 77.0 % (Table 4-7).

57

Table 4-7 The removal rate constants, removal efficiencies and debromination efficiencies of TBBPA by Cu/Fe nanoparticles at various solution pH

Initial pH	Final pH	k (min^{-1})	Removal efficiency (%)	Br$^-$ concentration (μM)	Debromination efficiency (%)
3.0	8.19	0.162	99.0	37.1	100.8
5.0	8.67	0.228	99.7	34.9	94.8
7.0	8.54	0.204	99.4	36.7	99.7
9.0	8.74	0.191	98.7	30.8	83.6
11.0	10.87	0.063	77.0	11.5	31.3

The debromination efficiencies were over 80 % in different pH solutions except pH 11.0 (Table 4-7). Chen et al. (2001) showed that the H$^+$ was consumed during dehalogenation by NZVI, which indicated the reaction favors an acid condition. They also reported that the solution pH increased that resulted in the dechlorination of trichloroethylene by NZVI decreased. Our final pH changed to 8.19, 8.67, 8.54, 8.74, and 10.87 for pH 3.0, 5.0, 7.0, 9.0, and 11.0.

Figure 4-20 showed the effect of pH on the degradation and adsorption of TBBPA after 20 minutes reaction, most TBBPA molecules were removed by Cu/Fe nanoparticles with degradation at pH 3.0 to pH 9.0. However, at pH 11.0, the lowest removal efficiency as observed and over 20 % TBBPA adsorbed by Cu/Fe nanoparticles. Under slightly acidic condition (about pH 5.0), the iron oxides on the bimetallic particle were dissolved that reducing the passivation of metal; furthermore, the active sites of the particles surface was unlocked that facilitating direct contact of Fe^0 with halogenated organic compounds and exposing Fe^0 to contaminants (Satapanajaru et al., 2003; Zhang et al., 2006; Li et al.,2016). Moreover, at low pH

58

values, more ferrous (Fe^{2+}) and the hydrogen (or hydrogen atoms) were produced fast

in solution, and both Fe^{2+} and hydrogen are strong electron donors that accelerated the

dehalogenation (Zhang et al., 2006; Li et al., 2016).
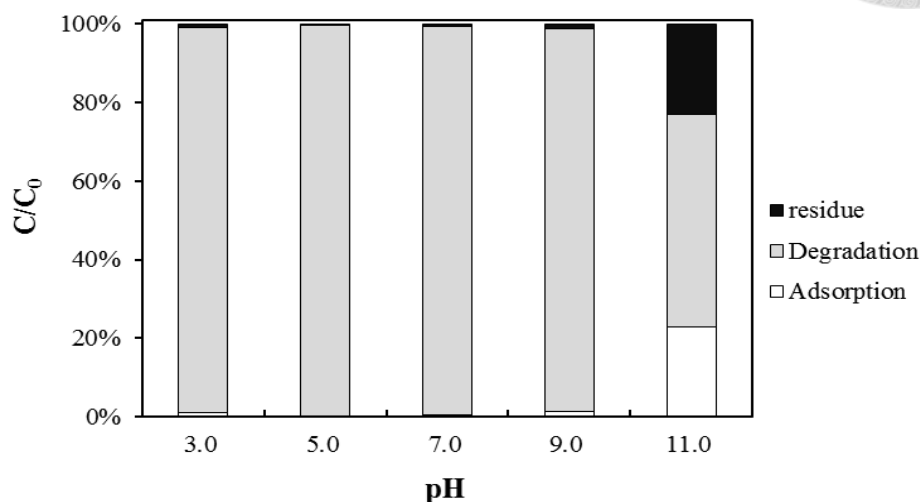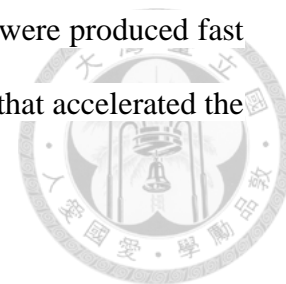
Figure 4-20 Effect of pH on the degradation and adsorption of TBBPA reacted with

Cu/Fe nanoparticles after 20 min reaction.

Figure 4-21 showed the time dependent concentration profiles for the intermediates

and final product at five initial pHs. During reaction, tribromobisphenol A

(tri-BBPA), dibromobisphenol A (di-BBPA), monobromo- bisphenol A

(mono-BBPA) and bisphenol A (BPA) were observed that were accompanied by

TBBPA removal. The concentration of three intermediates products increased first to

the maxima in sequence from three brominated compound to one brominated

compound, and then decreased with time. At low pH, TBBPA decreased more rapid,

and the intermediates increased and subsequently decreased faster (Figure 4-21). At

high pH, the intermediates increased and subsequently decreased slowly. Especially,

at an alkaline condition, it needed more time for the intermediate rose to the maxima

(Figure 4-21e). Due to the mono-BBPA, di-BBPA and tri-BBPA were not available

59

commercially, their concentrations in aqueous phase were determined from the chromatogram peak areas on a mass basis with compensation for the number of bromine based on the standard curves of TBBPA and BPA (Huang et al., 2013; Li et al., 2016). It might cause the loss of mass balance.

Figure 4-21 Time dependent concentration profiles for the intermediates and final product at initial solution pH: (a) 3.0, (b) 5.0, (c) 7.0, (d) 9.0, and (e) 11.0. The reaction solutions initially contained 2.0 g/L of Cu/Fe particles and 5.0 mg/L of TBBPA.

60

4.7 The surface property change of Cu/Fe nanoparticles after reaction

The XRD pattern of the synthesized Cu/Fe nanoparticles after reactions with TBBPA was shown in Figure 4-5. After reaction, the reacted Cu/Fe eventually showed the diffraction peaks of ion oxides and copper oxides but no Fe^0 and Cu^0 (Shih et al., 2016).

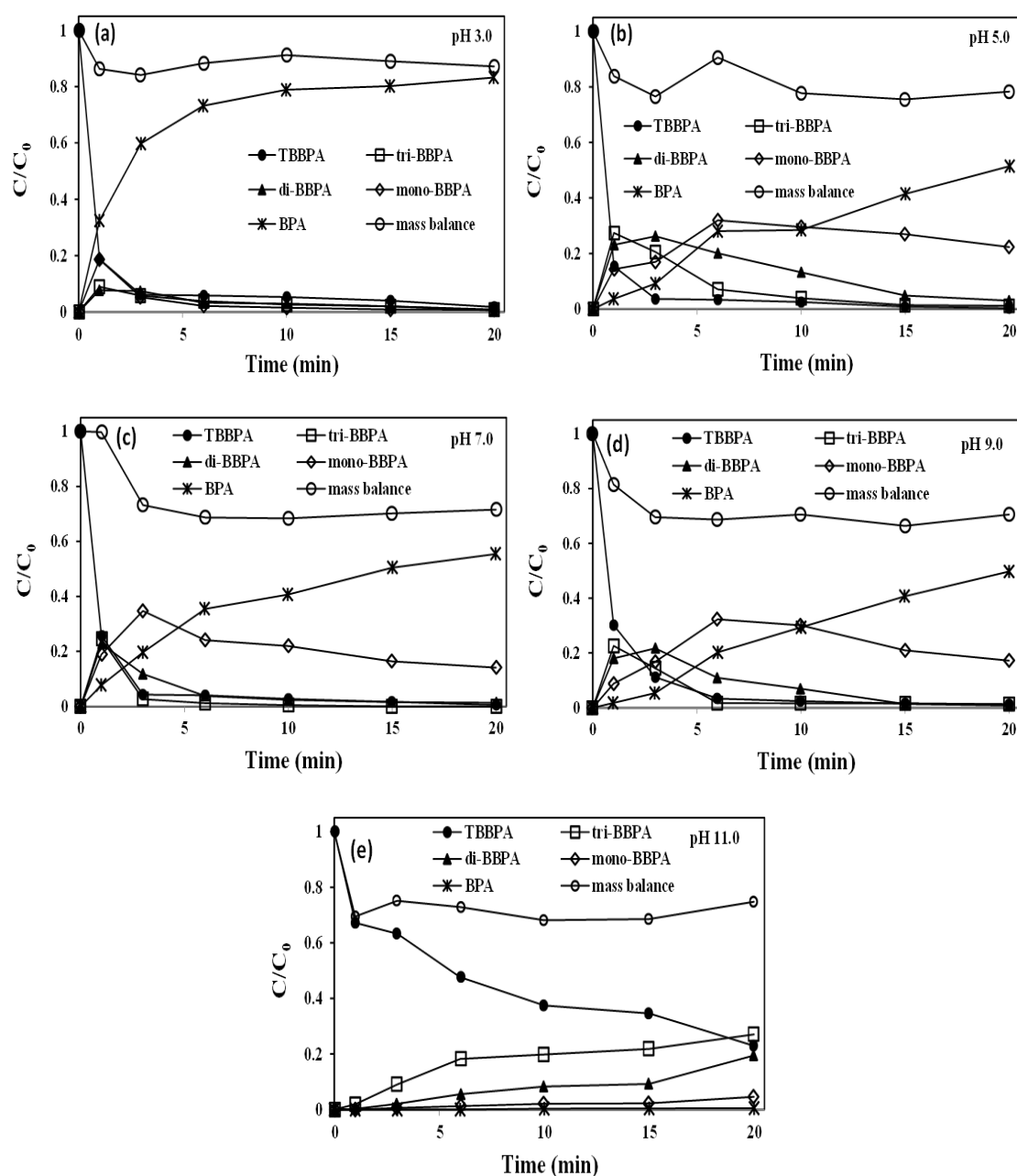Normalized Fe K-edge XANES was used to determine the speciation of iron in synthesized Cu/Fe nanoparticles after reaction (Figure 4-6). For Cu/Fe nanoparticles after reaction, the fraction of zero valent iron and iron oxides were about 65.2 % and 34.8 %, respectively (Table 4-1). The results indicated that these Cu/Fe nanoparticles before and after reaction were most zero valent iron, while including iron oxide after reacted TBBPA. The result differed from XRD with the occurrence of iron oxides. From the XRD pattern, there were no Fe^0 peaks being seen after reaction, which could be caused by the oxygen and TBBPA reacted with the synthesized nanoparticles in the solution. Also, the synthesized nanoparticles were oxidized in the ambient environment during the analysis, because it took much longer time for XRD analysis than XANES.

From the results of the linear combination fitting of Cu K-edge XANES spectra of Cu/Fe nanoparticles after reaction, the fraction of zero valent copper, Cu_2O and CuO were about 23.3 %, 54.7 %, and 22.1 %, respectively (Table 4-2). The results indicated that more copper oxide would appear after Cu/Fe nanoparticles react with TBBPA. After reaction, the oxidation state of Cu/Fe nanoparticles existed.

Figure 4-8 showed the Raman spectra of Cu/Fe nanoparticles at various pH conditions. There are no obvious iron oxides before reaction, but after reaction, geothite (FeOOH) and magnetite (Fe_3O_4) were observed at pH 7.0 and pH 11.0

61

respectively (Oh et al, 1998; Hanesch, 2009; Das and Hendry, 2011). It could make the TBBPA and its byproducts of degradation adsorbed on the nanoparticles.

4.8 The proposed debromination pathways of TBBPA by Cu/Fe nanoparticles

The proposed debromination pathway of TBBPA by Cu/Fe nanoparticles is shown in Figure 4-22. Figure 4-21 shows the time dependent concentration profiles for the intermediates and final product that were detected by HPLC. Only TBBPA and BPA could be identified by HPLC from the available standards. In order to identified these intermediates, HRESI/MS was used. From the HRESI/MS results, tri-BBPA, di-BBPA, and mono-BBPA were identified (Figure 4-23). The degradation products of TBBPA were identified as tri-BBPA, di-BBPA, and mono-BBPA. The proposed debromination pathway of TBBPA by Cu/Fe nanoparticles was in accordance our analysis, which is consistent with previous studies that degraded TBBPA by other iron-based bimetallic nanoparticles (Huang et al., 2013; Li et al., 2016).
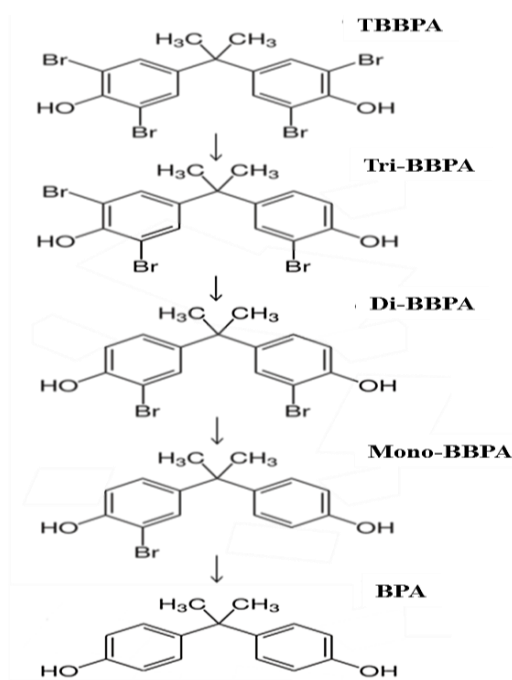
Figure 4-22. The debromination pathway of TBBPA by Cu/Fe nanoparticles.

62
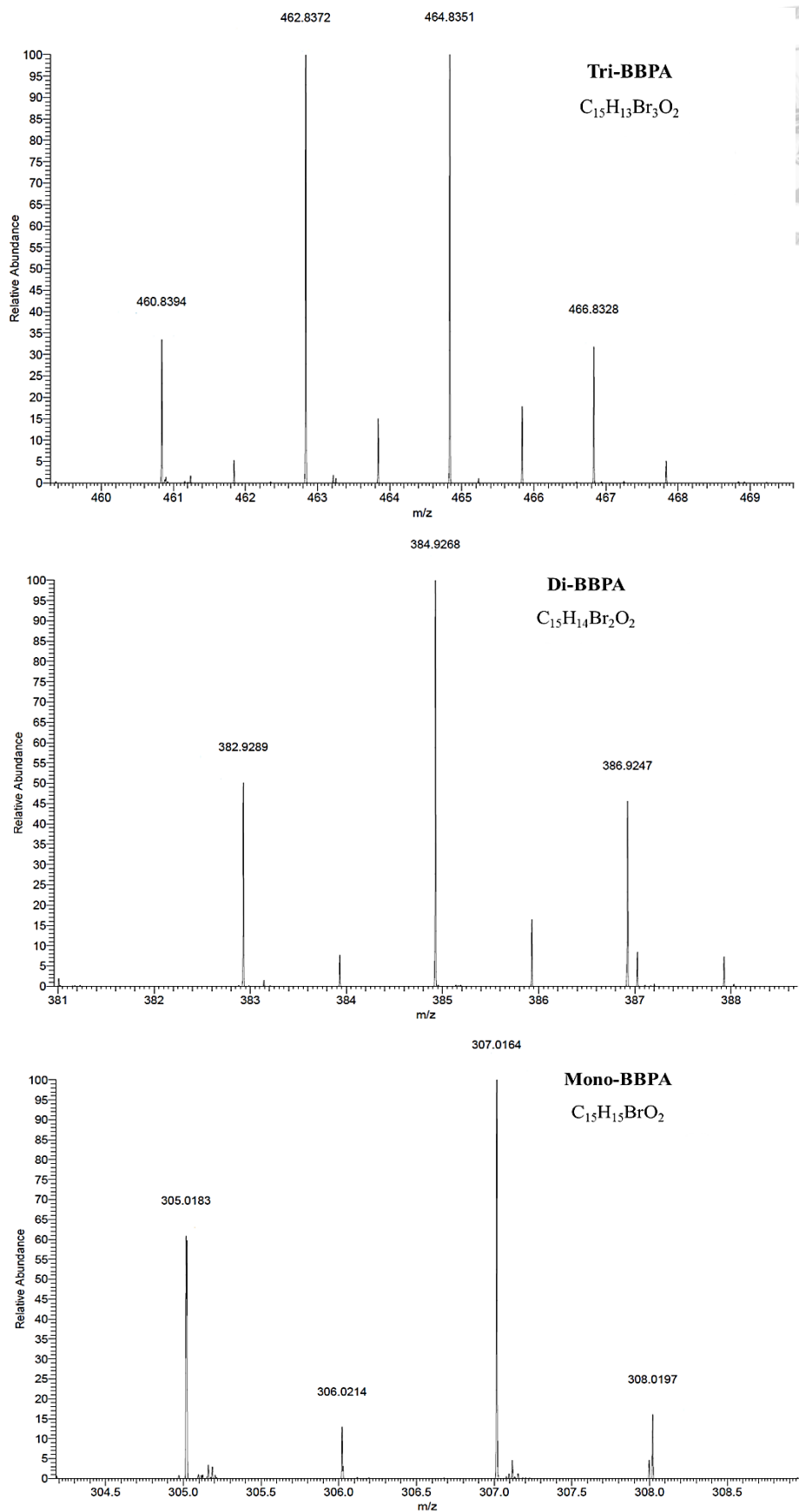
Figure 4-23. HRESI/MS chromatogram of TBBPA degradation intermediates.

4.9 Effect of H_2O_2 concentration on the removal of BPA by Fenton reaction

After TBBPA was debrominated by Cu/Fe nanoparticles, the solution contained methanol that acts as a cosolvent but consumes oxidants such as hydroxyl radicals and decrease the BPA degradation. In order to clearly understand the effect of H_2O_2 concentration on the BPA removal by Fenton reaction with specific concentration of Fe^{2+} and easy to operate experiments, no extra methanol was added into the reaction to avoid the competition for hydroxyl radicals between BPA and methanol. The initial concentrations of BPA, Fe^{2+} and pH value are 5.0 mg/L, 0.25 mM and 3.0, respectively. Three various concentrations of H_2O_2 at 0.025, 0.25, and 2.5 mM, were used to testify the degradation ability.

As shown in Figure 4-24, the concentration of H_2O_2 increased from 0.025mM to 0.25 mM, the BPA concentrations drop obviously.

Figure 4-24 Effect of H_2O_2 concentration on the removal of BPA by Fenton reaction (The reaction solutions contained 0.25 mM Fe^{2+} and 5.0 mg/L of BPA).

The removal rate constant increased with the concentration of H_2O_2 increased (Figure 4-25). The removal rate constants were 0.0004, 0.015, and 0.0107 min^{-1} for 0.025, 0.25, and 2.5 mM H_2O_2, respectively. The removal efficiencies were 4.3 %, 71.4

64

%, and 61.6 % for 0.025, 0.25, and 2.5 mM H_2O_2, respectively. Increasing the H_2O_2 concentration increased the removal rate and removal efficiency due to more hydroxyl radicals generated when H_2O_2 concentration increased. The results are consistent with a previous removal of 4-chloro-3-methyl phenol with Fenton reaction (Xu and Wang, 2011). However, increasing the H_2O_2 concentration to 2.5 mM, the BPA removal rate decreased. The reason is that H_2O_2 could complete with BPA for hydroxyl radicals for a high H_2O_2 concentration according to following equation (Daud and Hameed, 2010; Xu and Wang, 2011):

$$HO\cdot + H_2O_2 \rightarrow HO_2\cdot /O_2\cdot^- + H_2O \qquad (4\text{-}1)$$

The generated radicals ($HO_2\cdot$ and $O_2\cdot^-$) are weak to perform further oxidation (Liao et al., 2009; Daud and Hameed, 2010).
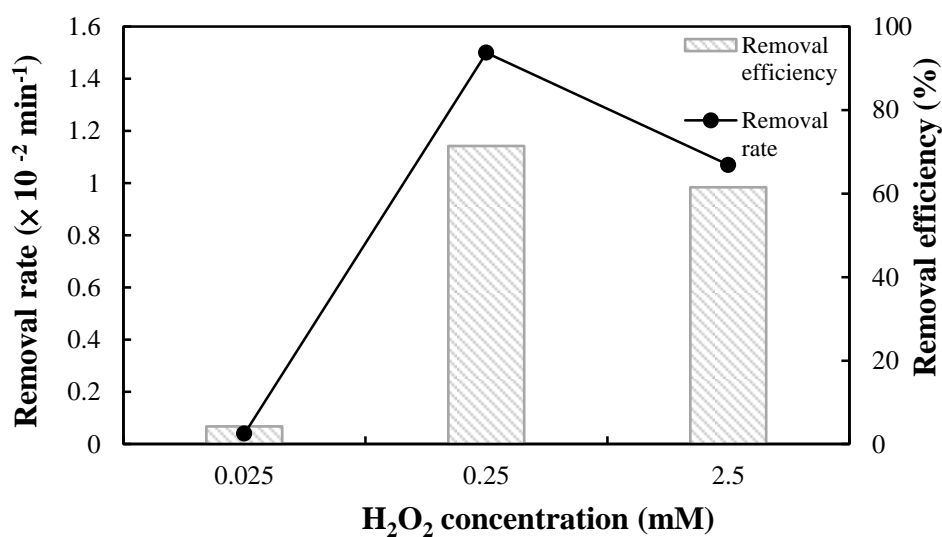
Figure 4-25 The rate constants and removal efficiency for the removal of BPA by Fenton reaction with various concentration of H_2O_2 (The reaction solutions contained 0.25 mM Fe^{2+} and 5.0 mg/L of BPA).

The mineralization of BPA with various concentration of H_2O_2 was shown in Figure 4-26. Increasing the H_2O_2 concentration, the mineralization increased in the

65

range of 0.025 mM to 0.25 mM (Shih and Tso, 2012). The TOC removal efficiencies were 12.8 %, 26.0 %, 44.6 %, and 10.7 % for 0.025, 0.1, 0.25, and 2.5 mM, respectively.
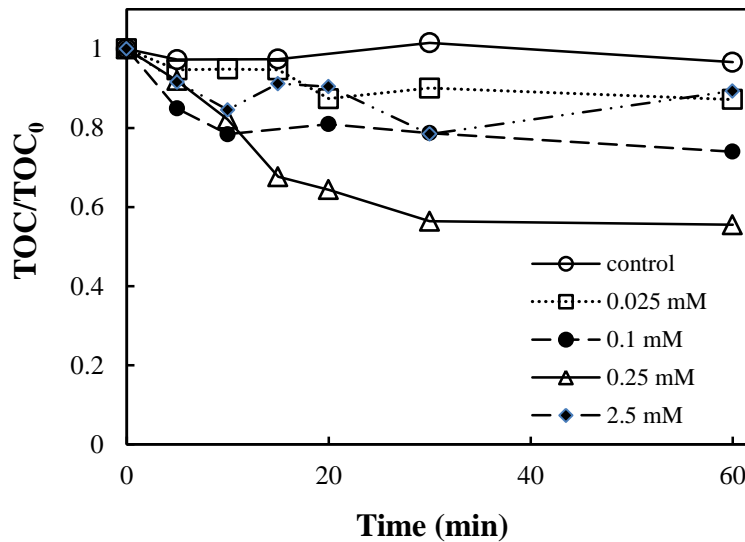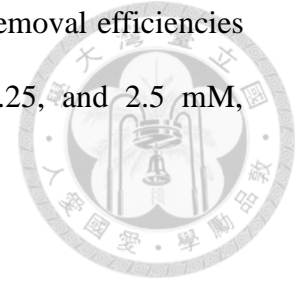
Figure 4-26 The mineralization of BPA by Fenton reaction with various concentration of H_2O_2

4.10 Effect of Fe^{2+} concentration on the removal of BPA by Fenton reaction

Four batch experiments were operated to investigate the effect of Fe^{2+} concentration on the removal of BPA. The initial concentrations of BPA, H_2O_2 and pH value are 5.0 mg/L, 0.25 mM and 3.0, respectively. Four various concentrations of Fe^{2+} were 0.025, 0.1, 0.25, and 2.5 mM, respectively .

As shown in Figure 4-27, the concentration of Fe^{2+} increased in the range of 0.025 to 0.25 mM, the BPA concentrations drop faster.
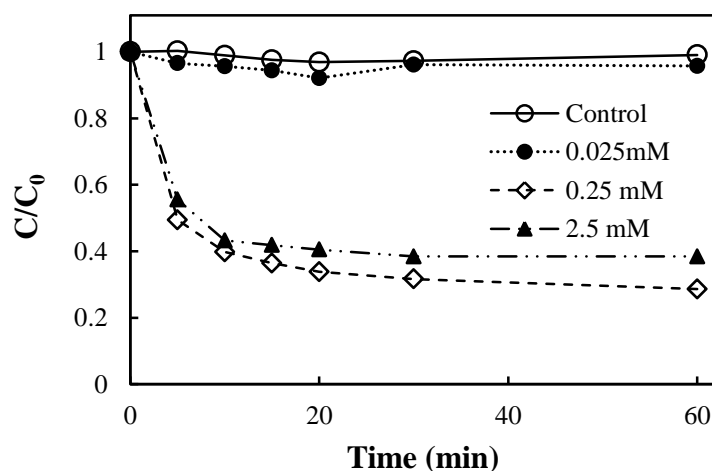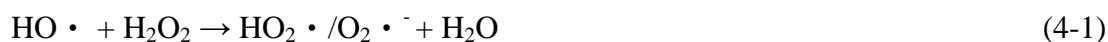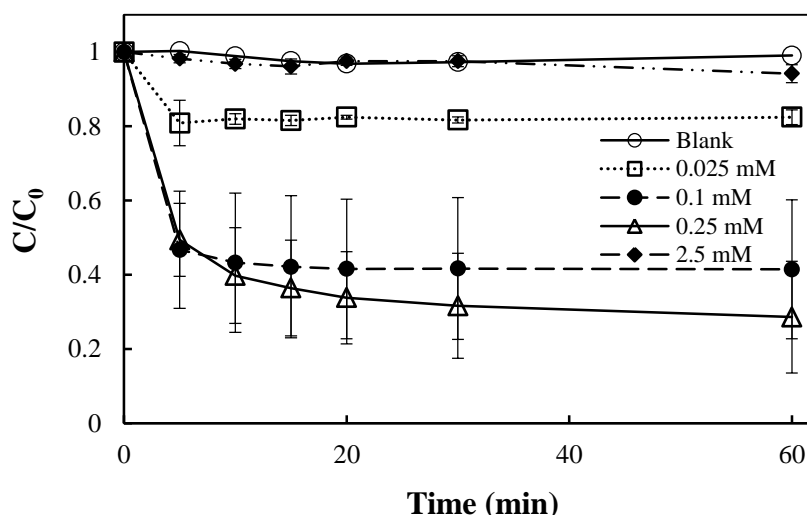
Figure 4-27 Effect of Fe^{2+} concentration on the removal of BPA by Fenton reaction (The reaction solutions contained 0.25 mM H_2O_2 and 5.0 mg/L of BPA).

The removal rate constant, removal efficiency and TOC removal efficiency increased with the concentration of Fe^{2+} increased in the range of 0.025 to 0.25 mM firstly, and drop dramatically when the concentration of Fe^{2+} increased up to 2.5 mM (Figure 4-28 and Figure 4-29). The removal rate constants were 0.0014, 0.0081, 0.015, and 0.0006 min^{-1} for 0.025, 0.1, 0.25, and 2.5 mM Fe^{2+}, respectively. The removal efficiencies were 15.6 %, 58.5 %, 71.4%, and 4.4 % for 0.025, 0.1, 0.25, and 2.5 mM Fe^{2+}, respectively. Increasing the Fe^{2+} concentration increased the removal rate and removal efficiency due to more hydroxyl radicals generated when Fe^{2+} concentration increased. The result are similar as a previous report (Sun et al., 2011). However, at a high concentration of Fe^{2+} with 2.5 mM, the removal rate and removal efficiency drop.

67

Some studies have revealed that the scavenge of hydroxyl radicals will occur with a

high concentration of Fe^{2+} according to following equation:

$$\cdot OH + Fe^{2+} \rightarrow Fe^{3+} + OH^- \tag{4-2}$$

Due to the oxidation of Fe^{2+}, the degradation behavior decreased (Joseph et al., 2000).
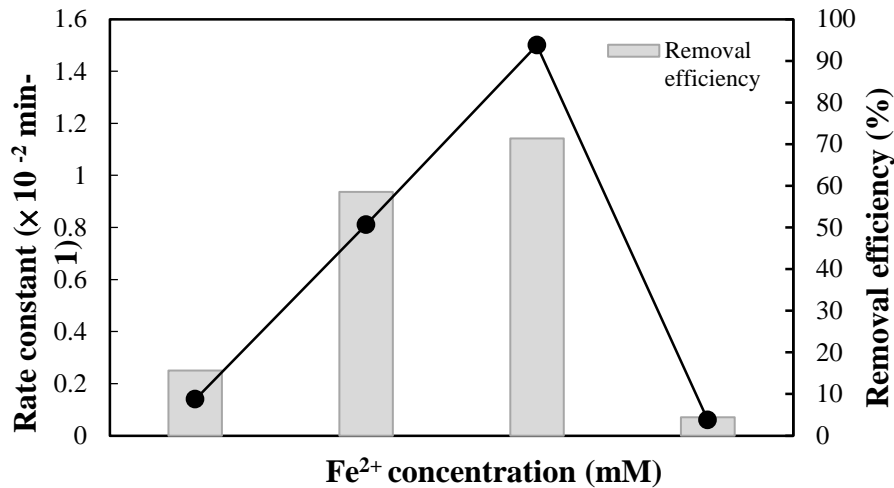
Figure 4-28 The rate constant and removal efficiency for the removal of BPA by Fenton reaction with various concentrations of Fe^{2+} (The reaction solutions contained 0.25 mM H_2O_2 and 5.0 mg/L of BPA).
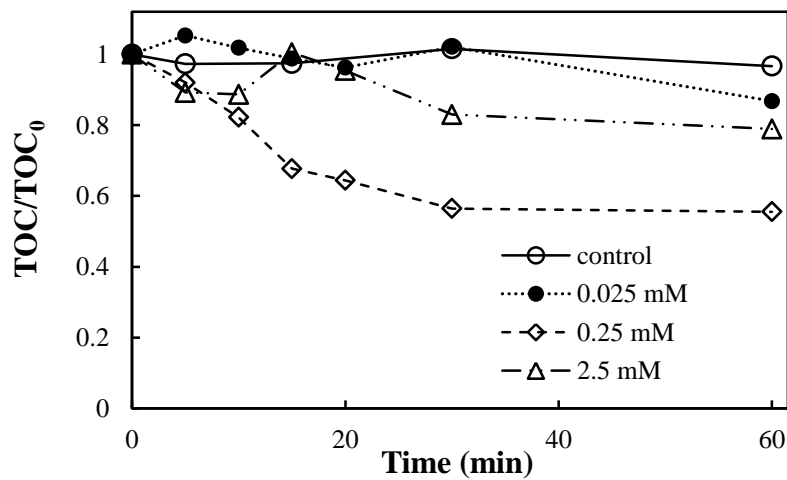
Figure 4-29 The mineralization of BPA by Fenton reaction with various concentration

of Fe^{2+}

68

Chapter 5 Conclusions
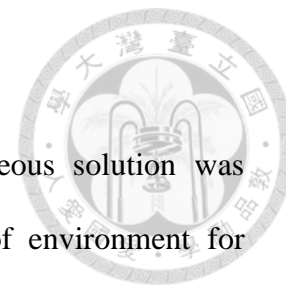
The removal of TBBPA with Cu/Fe nanoparticles in aqueous solution was evaluated to demonstrate the applicability in the remediation of environment for polyhalogenated aromatic contaminants. The increase of copper loading percentage enhanced the debromination efficiency of TBBPA from 0.5 % to 4 %; however, the debromination efficiency decreased as the copper ratio increased to 8 %. The most suitable copper content was 4 % with the highest removal rate constant of 0.229 min^{-1}. A higher dosage of Cu/Fe nanoparticles with more surface area could contact with TBBPA, suggesting more reactive sites on the nanoparticles could react with TBBPA and accelerate the removal of TBBPA. For the initial concentration of TBBPA, when increased the TBBPA concentration, the removal rate decreased in the range of 1.0 to 15.0 mg/L of TBBPA. However, all the debromination efficiencies were close 95 %, and it indicated that TBBPA was debrominated effectively by the Cu/Fe nanoparticles with the dosage of 2 g/L. The removal rate increased with the temperature increased from 5 $^{\circ}$C to 45 $^{\circ}$C and the activation energy of the removal reactions of TBBPA with Cu/Fe BNPs was 35.64 kJ/mole. This indicated that the removal of TBBPA by Cu/Fe BNPs is surface-control mechanism. The pH values played an important role on the removal of TBBPA. TBBPA removal favored slight acid conditions, and in the acid condition, the higher removal constant was observed because the passivation with iron oxide or iron hydroxide would be washed out and exposed the reactive sites. On the contrary, in the alkaline condition, the lower removal constant could be estimated and debromination efficiency would be inhibited owing to the passivated surface of these nanoparticles.

The debromination intermediates were identified and the bromide ions released

into solution were detected, which revealed that the Cu/Fe nanoparticles could debrominate TBBPA. TBBPA sequentially debrominated to tri-BBPA, di-BBPA, mono-BBPA, and BPA by nanoparticles. One bromide would be loss at each step during the debromination. The debromination pathways are presented.

The Fenton reaction exhibited a powerful ability for removing TBBPA debrominated byproduct in aqueous solution. The removal rate was affected by many factors, such as the initial concentrations of H_2O_2 and Fe^{2+}. Increasing the concentration of H_2O_2 in the range of 0.025 to 0.25 mM, the removal rate increased from 0.0004 to 0.015 min^{-1}. Besides, the removal efficiency also increased to 71.4 % with the concentration of H_2O_2 increased to 0.25 mM. Increasing the concentration of Fe^{2+} in the range of 0.025 to 0.25 mM, the removal rate increased from 0.0014 to 0.015 min^{-1}. A higher concentration of H_2O_2 or Fe^{2+} could complete with BPA for hydroxyl radical, that cause the BPA removal rate constant drop dramatically. The results demonstrate our synthesized Cu/Fe bimetallic nanoparticles have a high potential for TBBPA treatment and the final TBBPA debrominated byproduct could be removed effectively by a further Fenton reaction.

Reference

ACC (American Chemistry Council). Determination of effects on the growth of the common mussel *Mytilus edulis*. **2005**.

ACC-BFRIP (American Chemistry Council Brominated Flame Retardant Industry Panel). Tetrabromobisphenol A: A toxicity test to determine the effects of the test substance on seedling emergence of six species of plants. **2002.**

ACC-BFRIP (American Chemistry Council - Brominated Flame Retardants Industry Panel). Tetrabromobisphenol-A (TBBPA): A prolonged sediment toxicity test with *Hyalella azteca* using spiked sediment. **2006**.

Bao, Y.; Niu, J. Photochemical transformation of tetrabromobisphenol A under simulated sunlight irradiation: kinetics, mechanism and influencing factors. *Chemosphere* **2015**, 134, 550−556.

Bokare, A.D.; Chikate, R.C.; Rode, C.V.; Paknikar, K.M. Iron-nickel bimetallic nanoparticles for reductive degradation of azo dye Orange G in aqueous solution. *Appl. Catal. B: Environ.* **2008**, 79, 270-278.

Brezonik, P.L. (**1994**). Chemical kinetics and process dynamics in aquatic systems. Lewis Publishers.

Brown, D.D.; Wang, Z.; Furlow, J.D.; Kanamori, A.; Schawartzman, R.A.; FRemo B.F.; Pinder, A. The thyroid hormone-induced tail resorption program during xenopus laevis metamorphosis. *Developmental Biology* **1996**, 93, 1924-1929.

BSEF (Bromine Science and Environmental Forum). Major brominated flame retardants volume estimates. Total Market Demand by Region in 2001. **2001**, available at: http://www.bsef-site.com/docs/BFR_vols_2001.doc

BSEF (Bromine Science and Environmental Forum). **2006**, available at: http://www.bsef.com/bromine/faq/index.php

Cariou, R.; Antignac, J. P.; Zalko, D.; Berrebi, A.; Cravedi, J. P.; Maume, D.; Marchand, P.;Monteau, F.; Riu, A.; Andre, F.; Le Bizec, B. Exposure assessment of French women and their newborns to tetrabromobisphenol-A: occurrence measure-ments in maternal adipose tissue, serum, breast milk and cord serum. *Chemosphere* **2008**, 73, 1036-1041.

Chamarro, E.; Marco, A.; Esplugas, S. Use of Fenton reagent to improve organic chemical biodegradability. *Water Res.* **2001**, 35 (4), 1047-51.

Chan, W.K.; Chan, K.M. Disruption of the hypothalamic-pituitary-thyroid axis in zebrafish embryo–larvae following waterborne exposure to BDE-47, TBBPA and BPA. *Aquat. Toxicol.* **2012**, 108, 106–111

Chang, B.V.; Yuan, S.Y.; Ren, Y.L. Aerobic degradation of tetrabromobisphenol-A by microbes in river sediment. *Chemosphere* **2012**, 87, 535-541.

Chen, J.L.; Al-Abed, S.R.; Ryan, J.A.; Li, Z.B. Effects of pH on dechlorination of trichloroethylene by zero-valent iron. *J. Hazard. Mater.* **2001**, 83, 243-254

Chatterjeea, S.; Limb, S.R.; Woo, S.H. Removal of Reactive Black 5 by zero-valent iron modified with various surfactants. *Chem. Eng. J.* **2010**,160 (1), 27-32.

Covaci, A.; Voorspoels, S.; Abdallah, M.A.; Geens, T.; Harrad, S.; Law, R.J. Analytical and environmental aspects of the flame retardant tetrabromobisphenol-A and its derivatives. *J. Chromatogr. A* **2009**, 1216, 346–363.

Cwiertny, D.M.; Bransfield, S.J.; Roberts, A.L. Influence of the oxidizing species on the reactivity of iron-based Bimetallic reductants. *Environ. Sci. Technol.* **2007**, 15, 41 (10), 3734-3740.

Das, S.; Hendry, M. J. Application of Raman spectroscopy to identify iron minerals commonly found in mine wastes. *Chem. Geol.* **2011**, 290 (3–4), 24, 101–108.

Darnerud, P. O. Toxic effects of brominated flame retardants in man and in wildlife. *Environ. Int.* **2003**, 29, 841–853.

De Wit, C.A.; Herzke, D.; Vorkamp, K. Brominated flame retardants in the Arctic environment - trends and new candidates. *Sci Total Environ.* **2010**, 408, 2885–2918.

Decherf, S.; Seugnet, I.; Fini, J.B.; Clerget-Froidevaux, M.S.; Demeneix, B.A. Disruption of thyroid hormone-dependent hypothalamic set-points by environmental contaminants. *Mol. Cell. Endocrinol.* **2010**, 323 (2), 172-182.

Doong, R.A.; Saha, S.; Leeb, C.H.; Lin, H.P. Mesoporous silica supported bimetallic Pd/Fe for enhanced dechlorination of tetrachloroethylene. *RSC Adv.* **2015**, 5, 90797–90805

EC (European Commission). Risk Assessment of 2,2',6,6-Tetrabromo-4,4'-Isopropyl-idene Diphenol (Tetrabromobisphenol-A): CAS Number: 79-94-7; EINECS Number: 201-236-9; Final Environmental Rar of February 2008. R402_0802_ env. Rapporteur: United Kingdom. **2008**. http://echa.europa.eu/documents/ 10162/17c7379e-f47b-4a76-aa43-060da5830c07.

ECB (European Chemicals Bureau). European Union Risk Assessment Report - 2,2',6,6'-tetrabromo-4,4'-isopropylidenediphenol, (tetrabromobisphenol-A or TBBP-A) (CAS No: 79-94-7) Part II – human health. European Commission – Joint Research Centre, Institute for Health and Consumer Protection. Luxembourg: Office for Official Publications of the European Communities (**2006**) OEINECS No: 201-236-9. Series: 4th Priority List Volume: 63.

EFSA (European Food Safety Authority). EFSA panel on contaminants in the food chain (CONTAM): scientific opinion on Tetrabromobisphenol A (TBBPA) and its derivatives in food. *EFSA Journal* **2011**, 9 (12), 2477.

Elliott, D.W.; Zhang, W.X. Field assessment of nanoscale bimetallic particles for groundwater treatment. *Environ.Sci.Technol.* **2001**, 35, 4922-4926.

Fang Y.; Al-Abed S.R. Correlation of 2-chlorobiphenyl dechlorination by Fe/Pd with iron corrosion at different pH. *Environ. Sci. Technol.* **2008**, 15, 42 (18), 6942-6948.

Fang, Z.; Qiu, X.; Chen, J. Qiu, X. Debromination of polybrominated diphenyl ethers by Ni/Fe bimetallic nanoparticles: influencing factors, kinetics, and mechanism. *J. Hazard. Mater.* **2011**, 185 (2-3), 958-969.

Feng, J.; Lim, T.T. Pathways and kinetics of carbon tetrachloride and chloroform reductions by nano-scale Fe and Fe/Ni particles: comparison with commercial micro-scale Fe and Zn. *Chemosphere* **2005**, 59 (9), 1267–1277.

GC (Government of Canada). Screening Assessment Report on Phenol, 4,4'-(1-methylethylidene)bis[2,6-dibromo-, Ethanol, 2,2'-[(1-methylethy-lidene)bis-[(2,6-dibromo-4,1-phenylene)oxy]]bis, Benzene, 1,1'-(1-methylethylidene)bis-[3,5-dibromo-4-(2-propenyloxy)-. **2013**. Available at: http://www.ec.gc.ca/ese-ees/BEE093E4-8387-4790-A9CD-C753B3E5BFAD/FSAR_TBBPA_EN.pdf

George, K. W.; Häggblom, M. M. Microbial o-methylation of the flame retardant tetrabromobisphenol-A. *Environ. Sci. Technol.* **2008**, 42 (15), 5555–5561.

GLCC (Great Lakes Chemical Corporation). The acute toxicity of FMBP4A (Tetrabromobisphenol a) to the bluegill sunfish, *Lepomis macrochirus* Rafinesque. **1978a.**

GLCC (Great Lakes Chemical Corporation). The acute toxicity of FMBP4A (Tetrabromobisphenol a) to the rainbow trout, *Salmo gairdneri* Richardson. **1978b.**

GLCC (Great Lakes Chemical Corporation). Acute toxicity of tetrabromobisphenol a to fathead minnow (*Pimephales promelas*) under flow-through conditions. **1988a.**

Gorga, M.; Martínez, E.; Ginebreda, A.; Eljarrat, E.; Barceló, D. Determination of PBDEs, HBB, PBEB, DBDPE, HBCD, TBBPA and related compounds in sewage sludge from Catalonia (Spain). *Sci. Total Environ.* **2013**, 444,51-59.

Graham, L.J.; Jovanovic, G. Dechlorination of *p*-chlorophenol on a Pd/Fe catalyst in amagetically stabilized fluidized bed; Implications for sludge and liquid remediation. *Chem. Eng. Sci.* **1999**, 54 (15-16), 3085-3093.

Halldin, K.; Berg, C.; Bergman, A.; Brandt, I.; Brunström, B. Distribution of bisphenol A and tetrabromobisphenol A in quail eggs, embryos and laying birds and studies on reproduction variables in adults following in ovo exposure. *Arch Toxicol.* **2001**, 75 (10), 597-603.

Han, S.K.; Bilski, P.; Karriker, B.; Sik, R.H.; Chignell, C.F. Oxidation of flame retardant tetrabromobisphenol A by singlet oxygen. *Environ Sci Technol.* **2008**, 42 (1), 166-72.

Hanada, H.; Katsu, K.; Kanno, T.; Sato, E.F.; Kashiwagi, A.; Sasaki, J.; Inoue, M.; Utsumi, K. Cyclosporin an inhibits thyroid hormone-induced shortening of the tadpole tail through membrane permeability transition. *Comparative Biochemistry and Physiology. Part B.* **2003**, 135, 473-483.

Hanesch, M. Raman spectroscopy of iron oxides and (oxy)hydroxides at low laser power and possible applications in environmental magnetic studies. *Geophys. J. Int.* **2009**, 177, 941-948.

Harrad, S.; Abdallah, M.A.; Rose, N.L.; Turner, S.D.; Davidson, T.A. Current-use brominated flame retardants in water, sediment, and fish from English lakes. *Environ. Sci. Technol.* **2009**, 43 (24), 9077-9083.

He, M.J.; Luo, X.J.; Yu, L.H.; Wu, J.P.; Chen, S.J.; Mai, B.X. Diasteroisomer and enantiomer-specific profiles of hexabromocyclododecane and tetrabromo-bisphenol A in an aquatic environment in a highly industrialized area, South China: vertical profile, phase partition, and bioaccumulation. *Environ. Pollut.* **2013**, 179, 105-110.

Hendriks, H.S.; van Kleef, R. G. D. M.; van den Berg, M.; Westerink, R. H. S. Multiple novel modes of action involved in the in vitro neurotoxic effects of Tetrabromo-bisphenol-A. *Toxicol. Sci.* **2012**, 128 (1), 235-246.

Huang, C.C.; Lo, S.L.; and Lien, H.L. Vitamin B12-mediated hydrodechlorination of dichloromethane by bimetallic Cu/Al particles. *Chem. Eng. J.* **2015**, 273, 413-420.

Huang, Q.; Liub, W.; Peng, P.; Huang, W. Reductive debromination of tetrabromo-bisphenol A by Pd/Fe bimetallic catalysts. *Chemosphere* **2013**, 92 (10), 1321–1327

Huang, D.Y.; Zhao, H.Q.; Liu, C.P.; Sun, C.X. Characteristics, sources, and transport of tetrabromobisphenol A and bisphenol A in soils from a typical e-waste recycling area in South China. *Environ. Sci. Pol. Res.* **2014**, 21 (9), 5818–5826.

Jiang, C.; Pang, S.; Ouyang, F.; Ma, J., Jiang, J. A new insight into Fenton and Fenton-like processes for water treatment. *J. Hazard. Mater.* **2010**, 174 (1-3),813-817.

Johnson-Restrepo, B.; Adams, D.H.; Kannan, K. Tetrabromobisphenol A (TBBPA) and hexabromocyclododecanes (HBCDs) in tissues of humans, dolphins, and sharks from the United States. *Chemosphere* **2008**, 70 (11), 1935-1944.

Kashiwagi, A.; Hanada, H.; Yabuki, M.; Kanno, T.; Ishisaka, R.; Sasaki, J.; Inoue, M.;

Utsumi. K. Thyroxine enhancement and the role of reactive oxygen species in tadpole tail apoptosis. *Free. Radic. Biol. Med.* **1999**, 26, 1001-1009.

Kitamura, S.; Jinno, N.; Ohta, S.; Kuroki, H.; Fujimoto, N. Thyroid hormonal activity of the flame retardants tetrabromobisphenol A and tetrachlorobisphenol A. *Biochem. Biophys. Res. Commun.* **2002**, 293 (1), 554-559.

Koike, E.; Yanagisawa, R.; Takigami, H.; Takano, H. Brominated flame retardants stimulate mouse immune cells in vitro. *J. Appl. Toxicol.* **2013**, 33 (12),1451-1459.

Krueger, H. e. a.. Tetrabromobisphenol A: A prolonged sediment toxicity test with *Lumbriculus Variegatus* using spiked sediment with 2% total organic carbon. Wildlife International, Ltd. **2002a**.

Krueger, H. e. a. Tetrabromobisphenol A: A prolonged sediment toxicity test with *Lumbriculus variegatus* using spiked sediment with 5% total organic carbon Wildlife International, Ltd. **2002b.**

Li, Y.; Hsieh, W.P.; Mahmudov, R.; Weia, X.; Huang, C.P. Combined ultrasound and Fenton (US-Fenton) process for the treatment of ammunition wastewater. *J. Hazard. Mat.* **2013**, 244-245, 403-411.

Li, Y.; Li, X.; Xiao, Y.; Wei, C.; Han, D.; Huang, W. Catalytic debromination of tetrabromobisphenol A by Ni/nZVI bimetallic particles. *Chem. Eng. J.* **2016**, 284, 1242–1250

Li, F.; Wang, J.; Jiang, B.; Yang, X.; Nastold, P.; Kolvenbach, B.; Wang, L.; Ma, Y.; Corvini, P. F. X.; Ji, R. Fate of tetrabromobisphenol A (TBBPA) and formation of ester- and ether-linked bound residues in an oxic sandy soil. *Environ. Sci. Technol.* **2015**, 49 (21), 12758−12765.

Lien, H.L.; Zhang, W.X. Nanoscale iron particles for complete reduction of chlorinated ethenes. *Colloids Surf. A Physicochem. Eng. Asp*. **2011**, 191, 97-105.

Lien, H.L.; Zhang, W.X. Nanoscale Pd/Fe bimetallic particles: catalytic effects of palladium on hydrodechlorination. *Appl. Catal. B: Environ.* **2007**, 77, 110–116.

Lin, K.; Ding, J.F.; Huang, X.W. Debromination of tetrabromobisphenol A by nanoscale zerovalent iron: kinetics, influencing factors, and pathways. *Ind. Eng. Chem. Res.*, **2012**, 51 (25), 8378–8385.

Lin, K.; Liu, W.; Gan, J. Reaction of tetrabromobisphenol A (TBBPA) with manganese dioxide: kinetics, products, and pathways. *Environ. Sci. Technol.* **2009**, 43 (12), 4480−4486

Liu, G.B.; Zhao, H.Y.; Thiemann, T. Zn dust mediated reductive debromination of tetrabromobisphenol A (TBBPA). *J. Hazard. Mat.* **2009**, 169, 1150–1153.

Liu, J.; Wang, Y.; Jiang, B.; Wang, L.; Chen, J.; Guo, H.; Ji, R. Degradation, metabolism, and bound-residue formation and release of Tetrabromobisphenol A in soil during sequential anoxic-oxic incubation. *Environ. Sci. Technol.* **2013**, 47 (15), 8348-8354.

Liu, K.; Li, J.; Yan, S.; Zhang, W.; Li, Y.; Han, D. A review of status of tetrabromobisphenol A (TBBPA) in China. *Chemosphere* **2016**, 148, 8-20.

Lowry, G.V.; Johnson, K.M. Congener-specific dechlorination of dissolved PCBs by microscale and nanoscale zerovalent iron in a water/methanol solution. *Environ. Sci. Technol.* **2004**, 38, 5208–5216.

Lucas, M.S.; Peres, J.A. Decolorization of the azo dye Reactive Black 5 by Fenton and photo-Fenton oxidation. *Dyes and Pigments* **2006**, 71 (3), 236–244.

Luo, S.; Yang, S.G.; Wang, X.D.; Sun, C. Reductive degradation of tetrabromo-bisphenol A over iron-silver bimetallic nanoparticles under ultrasound radiation. *Chemosphere* **2010**, 79, 672.

Luo, S.; Yang, S.G.; Wang, X.D.; Sun, C. Reductive degradation of tetrabromo-bisphenol A using iron–silver and iron–nickel bimetallic nanoparticles with microwave energy. *Environ. Eng. Sci.* **2012**, 29, 453–460.

Matheson, L.J.; Tratnyek, P.G. Reductive Dehalogenation of Chlorinated Methanes by Iron Metal. *Environ. Sci. Technol.* **1994**, 28 (12), 2045–2053.

Matsukami, H.; Tue, N.M.; Suzuki, G.; Someya, M.; Tuyen, L.H.; Viet, P.H.; Takahashi, S.; Tanabe, S.; Takigami, H. Flame retardant emission from e-waste recycling operation in northern Vietnam: Environmental occurrence of emerging organophosphorus esters used as alternatives for PBDEs. *Sci. Total Environ.* **2015**, 514, 492–499.

McCormick J.M.; Paiva, M.S.; Häggblom, M.M.; Cooper, K.R.; White, L.A. Embryonic exposure to tetrabromobisphenol A and its metabolites, bisphenol A and tetrabromobisphenol A dimethyl ether disrupts normal zebrafish (Danio rerio) development and matrix metalloproteinase expression. *Aquat. Toxicol.* **2010**, 100 (3), 255-262.

Meerts, I.A.; van Zanden, J.J.; Luijks, E.A.; van Leeuwen-Bol, I.; Marsh, G.; Jakobsson, E.; Bergman, A.; Brouwer, A. Potent competitive interactions of some brominated flame retardants and related compounds with human transthyretin *in vitro*. *Toxicol. Sci.* **2000**, 56 (1), 95-104.

Moon, B.H.; Park, Y.B.; Park, K.H. Fenton oxidation of Orange II by pre-reduction using nanoscale zero-valent iron. *Desalination* **2011**, 268 (1-3), 249-252.

Morris, S.; Allchin, C.R.; Zegers, B.N.; Haftka, J.J.; Boon, J.P.; Belpaire, C.; Leonards, P.E.; Van Leeuwen, S.P.; De Boer, J. Distribution and fate of HBCD and TBBPA brominated flame retardants in North Sea estuaries and aquatic

food webs. *Environ. Sci. Technol.* **2004**, 38 (21), 5497-5504.

Nakajima, A.; Saigusa, D.; Tetsu, N.; Yamakuni, T.; Tomioka, Y; Hishinuma, T. Neurobehavioral effects of tetrabromobisphenol A, a brominated flame retardant, in mice. *Toxicol. Lett.* **2009**, 189, 78-83.

Neyens, E.; Baeyens, J. A review of classic Fenton's peroxidation as an advanced oxidation technique. *J. Hazard. Mater.* **2003**, 98, (1-3), 33-50.

Ni, H.G.; Zeng, H. HBCD and TBBPA in particulate phase of indoor air in Shenzhen, China. *Sci. Total Environ.* **2013**, 458-460, 15-19.

Nollet, L. M. L. Analysis of endocrine disrupting compounds in food. Blackwell Publishing Ltd. **2011**, 377-411.

Ogunbayo, O. A.; Michelangeli, F. The widely utilized brominated flame retardant tetrabromobisphenol A (TBBPA) is a potent inhibitor of the SERCA Ca^{2+} pump. *Biochem J.* **2007**, 408, 407–415.

Oh, S. J.; Cook, D.C.; Townsend, H.E. Characterization of iron oxides commonly formed as corrosion products on steel. *Hyperfine Interact.* **1998**, 112 (1), 59–66.

Osako, M.; Kim, Y.J.; Sakai, S. Leaching of brominated flame retardants in leachate from landfills in Japan. *Chemosphere* **2004**, 57 (10), 1571-1579.

Parshetti G.K.; Doong, R.A. Dechlorination of chlorinated hydrocarbons by bimetallic Ni/Fe immobilized on polyethylene glycol-grafted microfiltration membranes under anoxic conditions. *Chemosphere* 2012, 86 (4), 392-399.

Pimentel, M.; Oturan, N.; Dezotti, M.; Oturan, M.A. Phenol degradation by advanced electrochemical oxidation process electro-Fenton using a carbon felt cathode. *Appl. Catal. B: Environ.* **2008**, 83, 140–149.

Pullen, S.; Boecker, R.; Tiegs, G. The flame retardants tetrabromobisphenol A and tetrabromobisphenol A-bisallylether suppress the induction of interleukin-2–receptor alpha chain (CD25) in murine splenocytes. *Toxicology* **2003**, 184:11–22.

Puls, R.W.; Paul, C.J.; Powell, R. M. The application of in situ permeable reactive (zero-valent iron) barrier technology for the remediation of chromate-contaminated groundwater: a field test. *Appl. Geochem.* 1999, 14, 989-1000.

Qu, R.; Feng, M.; Wang, X.; Huang, Q.; Lu, J.; Wang, L.; Wang, Z. Rapid removal of tetrabromobisphenol A by ozonation in water: oxidation products, reaction pathways and toxicity assessment. *PLoS ONE* **2015**, 10 (10), 1-17.

Reistad, T.; Mariussen, E.; Ring, A.; Fonnum, F. In vitro toxicity of tetrabromo-bisphenol-A on cerebellar granule cells: cell death, free radical

formation, calcium influx and extracellular glutamate. *Toxicol. Sci.* **2007**, 96 (2), 268-278.

Ren, Y.L. Biodegradation of Tetrabromobisphenol A in river sediment. (Master's thesis, Soochow University, Taipei, Taiwan). 2010.

Ronen, Z.; Abeliovich, A. Anaerobic-aerobic process for microbial degradation of tetrabromobisphenol A. *Appl. Environ. Microbiol.* **2000**, 66 (6), 2372-2377.

Ronisz, D.; Finne, E. F.; Karlsson, H.; Förlin, L. Effects of the brominated flame retardants hexabromocyclododecane (HBCDD), and tetrabromobisphenol A (TBBPA), on hepatic enzymes and other biomarkers in juvenile rainbow trout and feral eelpout. *Aquat. Toxicol.* **2004**, 69, 229–245.

Satapanajaru, T.; Comfort, S.D.; Shea, P.J. Enhancing metolachlor destruction rates with aluminum and iron salts during zerovalent iron treatment. *J. Environ. Qual.* **2003**, 32 (5), 1726-1734.

Shi, Z.; Jiao, Y.; Hu, Y.; Sun, Z.; Zhou, X.; Feng, J.; Li, J.; Wu, Y. Levels of tetrabromobisphenol A, hexabromocyclododecanes and polybrominated diphenyl ethers in human milk from the general population in Beijing, China. *Sci. Total Environ.* **2013**, 452-453, 10-18.

Shih, Y.H.; Chen, M.Y.; Su, Y.F. Reduction of hexachlorobenzene by nanoscale zero-valent iron: Kinetics, pH effect, and degradation mechanism. *Separ. Sci. Technol.* **2011**, 76 (3), 268-274.

Shih, Y.H.; Chen, M.Y.; Su, Y.F.; Tso, C.P. Concurrent oxidation and reduction of pentachlorophenol by bimetallic zerovalent Pd/Fe nanoparticles in an oxic water. *J. Hazard. Mater.* **2016**, 301, 416–423.

Shih, Y.H.; Tso, C.P. Fast decolorization of azo-dye Congo Red with zerovalent iron nanoparticles and sequential mineralization with a fenton Reaction. *Environ. Eng. Sci.* **2012**, 29 (10), 929-933.

Smuleac, V.; Varma, R.; Sikdar, S.; Bhattacharyya, D. Green Synthesis of Fe and Fe/Pd Bimetallic Nanoparticles in Membranes for Reductive Degradation of Chlorinated Organics. *J. Memb. Sci.* **2011**, 379 (1-2), 131-137.

Song, H.; Carraway, E.R. Reduction of chlorinated ethanes by nanosized zero-valent iron: kinetics, pathways, and effects of reaction conditions. *Environ. Sci. Technol.* **2005**, 39 (16), 6237-6245.

Sun, Y.; Guo, H.; Yu, H.; Wang, X.; Wu, J.; Xue, Y. Bioaccumulation and physiological effects of tetrabromobisphenol A in coontail *Ceratophyllum demersum* L. *Chemosphere* **2008**, 70 (10), 1787-1795.

Sun, F.; Kolvenbach, B.A.; Nastold, P.; Jiang, B.; Ji, R.; Corvini, P.F. Degradation and metabolism of tetrabromobisphenol A (TBBPA) in submerged soil and soil-plant systems. *Environ. Sci. Technol.* **2014**, 48 (24), 14291-14299.

Sverdrup, L.E.; Hartnik, T.; Mariussen, E.; Jensen, J. Toxicity of three halogenated flame retardants to nitrifying bacteria, red clover (*Trifolium pratense*), and a soil invertebrate (*Enchytraeus crypticus*). *Chemosphere* **2006**, 64 (1), 96-103.

Szymanska, J. A.; Piotrowski, J. K.; Frydrych, B. Hepatotoxicity of tetrabromo-bisphenol-A: effects of repeated dosage in rats. *Toxicology* **2000**, 142, 87–95.

Tee, Y.H.; Grulke, E.; Bhattacharyya, B. Role of Ni/Fe nanoparticle composition on the degradation of trichloroethylene from water. *Ind. Eng. Chem. Res.* **2005**, 44 (18), 7062–7070.

Tian, H.; Li, J.J.; Mu, Z.; Li, L.D.; Hao, Z.P. Effect of pH on DDT degradation in aqueous solution using bimetallic Ni/Fe nanoparticles. *Sep. Purif. Technol.* **2009**, 66, 84–89.

Tso, C.P.; Shih, Y.H. The transformation of hexabromocyclododecane using zerovalent iron nanoparticle aggregates. *J. Hazard. Mater.* **2014**, 277, 76-83.

Tso, C.P.; Shih, Y.H. The reactivity of well-dispersed zerovalent iron nanoparticles toward pentachlorophenol in water. *Water Res.* **2015**, 72, 372-380.

USEPA (US Environmental Protection Agency). TSCA work plan chemical problem formulation and initial assessment. Tetrabromobisphenol A and related chemicals cluster flame retardants. **2015**. Available at: https://www.epa.gov/sites/production/files/2015-9/documents/tbbpa_problem_formulation_august_2015.pdf

Veldhoen, N.; Boggs, A.; Walzak, K.; Helbing, C.C. Exposure to tetrabromobisphenol-A alters TH-associated gene expression and tadpole metamorphosis in the Pacific tree frog *Pseudacris regilla*. *Aquat. Toxicol.* **2006**, 78 (3), 292–302.

Viberg, H.; Eriksson, P. Differences in neonatal neurotoxicity of brominated flame retardants, PBDE 99 and TBBPA, in mice. *Toxicology* **2011**, 289 (1), 59–65.

Vom Saal, F. S.; Nagel, S. C.; Coe, B. L.; Angle, B. M.; Taylor, J. A. The estrogenic endocrine disrupting chemical bisphenol A (BPA) and obesity. *Mol Cell Endocrinol*. **2012**, 354 (1-2), 74-84.

Waaijers, S.L.; Hartmann, J.; Soeter, A.M.; Helmus, R.; Kools, S.A.; de Voogt, P.; Admiraal, W.; Parsons, J.R.; Kraak, M.H. Toxicity of new generation flame retardants to *Daphnia magna*. *Sci. Total Environ.* **2013**,463-464, 1042-1048.

Wang X.; Chen, C.; Chang, Y.; Liu, H. Dechlorination of chlorinated methanes by Pd/Fe bimetallic nanoparticles. *J. Hazard. Mater.* **2009,** 161 (2-3), 815-823.

Wang, C.; Shih Y. Degradation and detoxification of diazinon by sono-Fenton and sono-Fenton-like processes. *Sep. Purif. Technol.* **2015**, 140, 6–12

Wang, J.; Liu, L.; Wang, J.; Pan, B.; Fu, X.; Zhang, G.; Zhang, L.; Lin, K.

Distribution of metals and brominated flame retardants (BFRs) in sediments, soils and plants from an informal e-waste dismantling site, South China. *Environ. Sci. Pollut. Res. Int.* **2015a**, 22 (2), 1020-1033.

Wang, W.; Abualnaja, K.O.; Asimakopoulos, A.G.; Covaci, A.; Gevao, B.; Johnson-Restrepo, B.; Kumosani, T.A.; Malarvannan, G.; Minh, T.B.; Moon, H.B.; Nakata, H.; Sinha, R.K.; Kannan, K. A comparative assessment of human exposure to tetrabromobisphenol A and eight bisphenols including bisphenol A via indoor dust ingestion in twelve countries. *Environ. Int.* **2015b**, 83, 183-191.

Wang, S.; Cao, S.; Wang, Y.; Jiang, B.; Wang, L.; Sun, F.; Ji, R. Fate and metabolism of the brominated flame retardant tetrabromobisphenol A (TBBPA) in rice cell suspension culture. *Environ. Pollut.* **2016**, 214, 299-306.

Wang, X.; Hu, X.; Zhang, H.; Chang, F.; Luo, Y. Photolysis kinetics, mechanisms, and pathways of tetrabromobisphenol A in water under simulated solar light irradiation. *Environ. Sci. Technol.* **2015c**, 49 (11), 6683−6690.

WHO (**1995**) Environmental health criteria 172. Tetrabromobisphenol A and derivatives. World Health Organization, Geneva.

Wojtowicz, A. K.; Szychowski, K. A.; Kajta, M. PPAR-γ agonist GW1929 but not antagonist GW9662 reduces TBBPA-induced neurotoxicity in primary neocortical cells. *Neurotox. Res.* **2014**, 25, 311–322.

Wollenberger, L.; Dinan, L.; Breitholtz, M. Effects of brominated flame retardants on two marine copepod species, *Acartia tonsa* and *Nitocra spinipes*, and on the Ecdysteroid-Responsive *Drosophila melanogaster* BII-Cell-Line. *Organohalogen Compounds* **2002**, 57, 451-454.

Watanabe, W.; Shimizu, T.; Sawamura, R.; Hino, A.; Konno, K.; Hirose, A.; Kurokawa, M. Effects of tetrabromobisphenol A, a brominated flame retardant, on the immune response to respiratory syncytial virus infection in mice. *Int. Immunopharm.* **2010**, 10, 393-397.

Xu, J.; Meng, W.; Zhang, Y.; Li, L.; Guo, C.S. Photocatalytic degradation of tetrabromobisphenol A by mesoporous BiOBr: Efficacy, products and pathway. *Appl. Catal. B: Environ.* **2011**, 107, 355-362.

Xu, L.; Wang, J.L. A heterogeneous Fenton-like system with nanoparticulate zero-valent iron for removal of 4-chloro-3-methyl phenol. *J. Hazard. Mater.* **2011**, 186, 256–264.

Yalfani, M.S.; Contreras, S.; Medina, F.; Sueiras, J. Phenol degradation by Fenton's process using catalytic in situ generated hydrogen peroxide. *Appl. Catal. B: Environ.* **2009**, 89 (3–4), 519–526.

Yang, S.; Wang, S.; Liu, H.; Yan, Z. Tetrabromobisphenol A: tissue distribution in fish,

and seasonal variation in water and sediment of Lake Chaohu, China. *Environ Sci. Pollut. Res. Int.* **2012**, 19 (9), 4090-4096.

Yuan, Y; Li, H.; Lai, B.; Yang, P.; Gou, M.; Zhou, Y.; Sun, G. Removal of high-concentration C.I. Acid Orange 7 from aqueous solution by zerovalent iron/copper (Fe/Cu) bimetallic particles. *Ind. Eng. Chem. Res.* **2014**, 53 (7), 2605–2613.

Zhang, Y.; Jing, L.Y.; He, X.H.; Li, Y.F.; Ma, X. Sorption enhancement of TBBPA from water by fly ash-supported nanostructured γ-MnO_2. *J. Ind. Eng. Chem.* 2015, 21, 610–619.

Zhang, W.X. Nanoscale iron particles for environmental remediation: an overview. *J. Nanopart. Res.* **2003**, 5, 323-332.

Zhang, W.; Quan, X.; Wang, J.; Zhang, Z.; Chen, S. Rapid and complete dechlorination of PCP in aqueous solution using Ni-Fe nanoparticles under assistance of ultrasound. *Chemosphere* **2006**, 65, 58-64.

Zheng, Z.H.; Yuan, S.H.; Liu, Y.; Lu, X.H.; Wan, J.H.; Wu, X.H.; Chen, J. Reductive dechlorination of hexachlorobenzene by Cu/Fe bimetal in the presence of nonionic surfactant. *J. Hazard. Mater.* **2009**, 170, 895–901.

Zhou, T.; Li, Y.; Ji, J.; Wong, F.S.; Lu, X. Oxidation of 4-chlorophenol in a heterogeneous zero valent iron/H_2O_2 Fenton-like system: kinetic, pathway and effect factors. *Sep. Purif. Technol.* **2008**, 62, 551–558.

Zhou, X.; Guo, J.; Zhang, W.; Zhou, P.; Deng, J.; Lin, K. Tetrabromobisphenol A contamination and emission in printed circuit board production and implications for human exposure. *J. Hazard. Mater.* **2014**, 273,27-35.

Zhu, N.; Luan, H.; Yuan, S.; Chen, J.; Wu, X.; Wang, L. Effective dechlorination of HCB by nanoscale Cu/Fe particles. *J. Hazard. Mater.* **2010,** 176, 1101–1105.

Zhuang, Y.; Ahn, S.; Seyfferth, A.L.; Masue-Slowey, Y.; Fendorf, S.; Luthy, R.G. Dehalogenation of polybrominated diphenyl ethers and polychlorinated biphenyl by bimetallic, impregnated, and nanoscale zerovalent iron. *Environ. Sci. Technol.* 2011, 45 (11), 4896-4903.

Zhuang, Y.; Jin, L.; Luthy, R.G. Kinetics and pathways for the debromination of polybrominated diphenyl ethers by bimetallic and nanoscale zerovalent iron: effects of particle properties and catalyst. *Chemosphere* **2012**, 89 (4), 426–432.

Appendix

VWD1 A, Wavelength=280 nm (KUO\2016-03-08 02-34-51 JOHN KUO-TBBPA\056-4201.D)

5 ppm TBBPA STD

VWD1 A, Wavelength=280 nm (KUO\2016-03-08 02-34-51 JOHN KUO-TBBPA\046-4101.D)

5 ppm STD BPA

VWD1 A, Wavelength=280 nm (KUO\2016-03-08 02-34-51 JOHN KUO-TBBPA\018-2201.D)
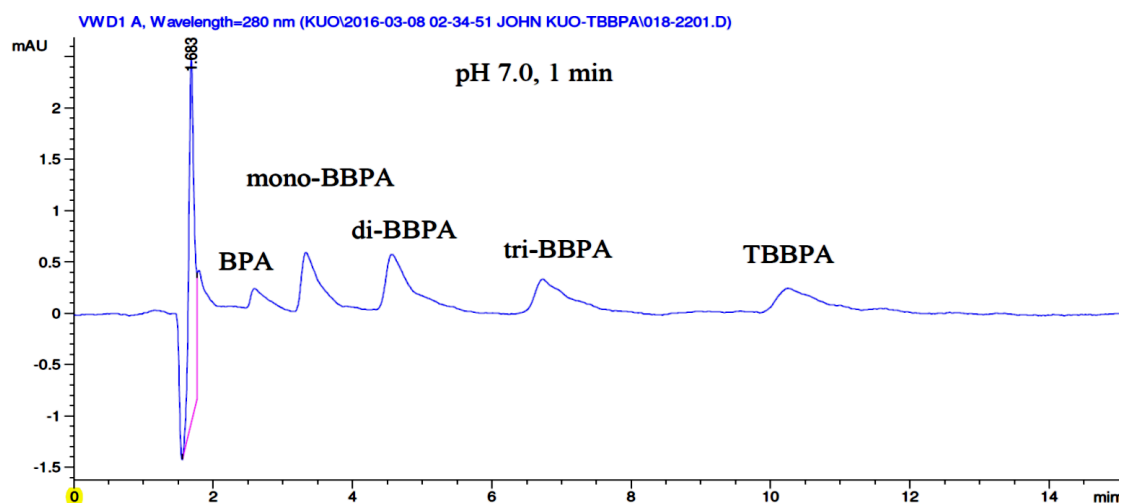
pH 7.0, 1 min

mono-BBPA
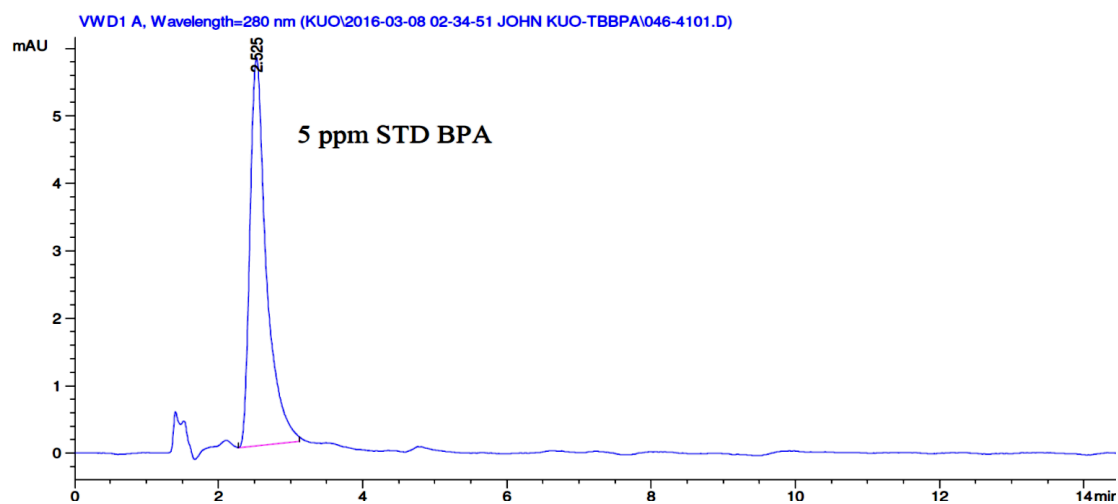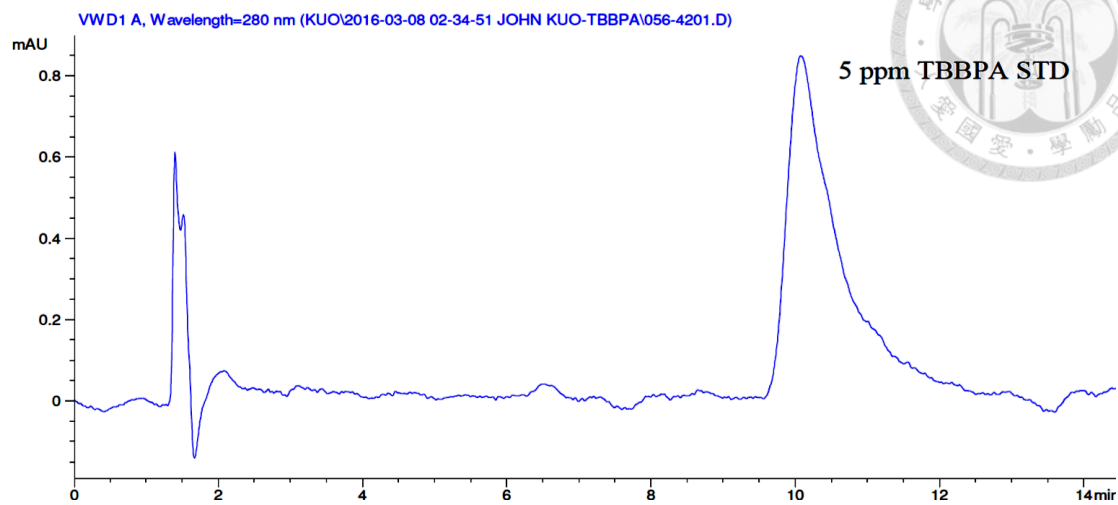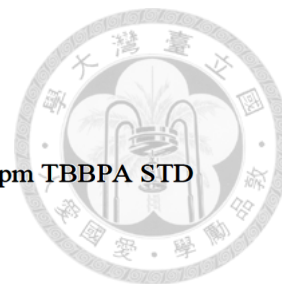
BPA

di-BBPA

tri-BBPA

TBBPA

Figure S1 HPLC chromatogram of TBBPA degradation intermediates and final product.
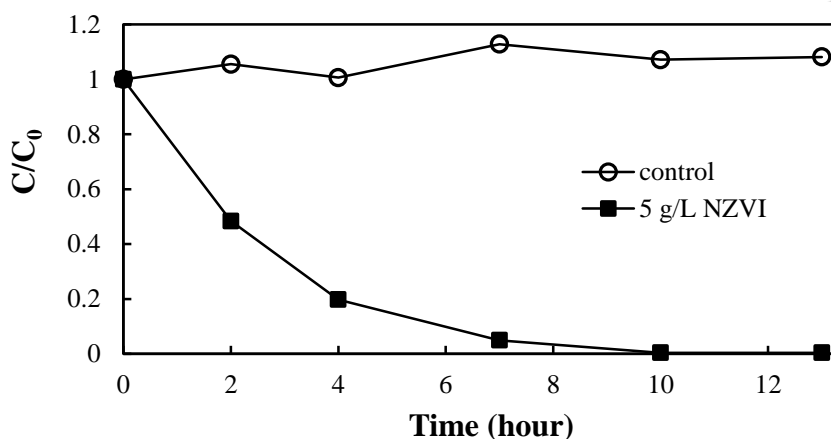
Figure S2 The kinetics of TBBPA removal by NZVI. (The reaction solutions contained 5.0 mg/L of TBBPA).
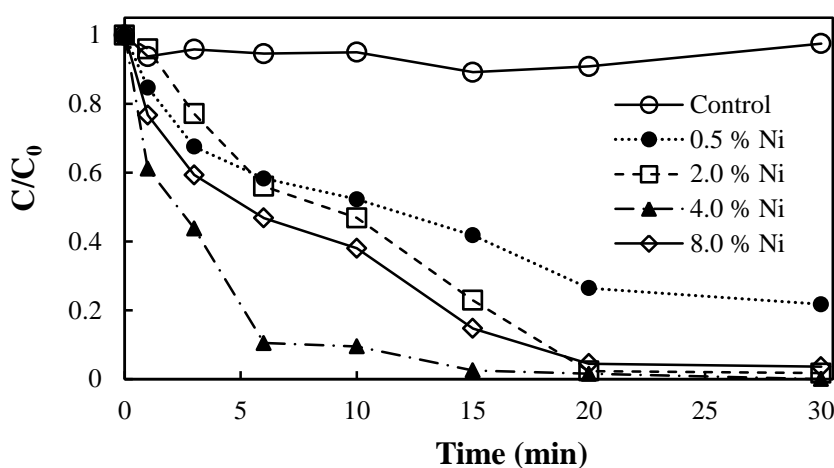

Figure S3 Effect of Ni content on the removal of TBBPA by Ni/Fe nanoparticles ([Ni/Fe]= 2.0 g/L and [TBBPA]=5.0 mg/L).
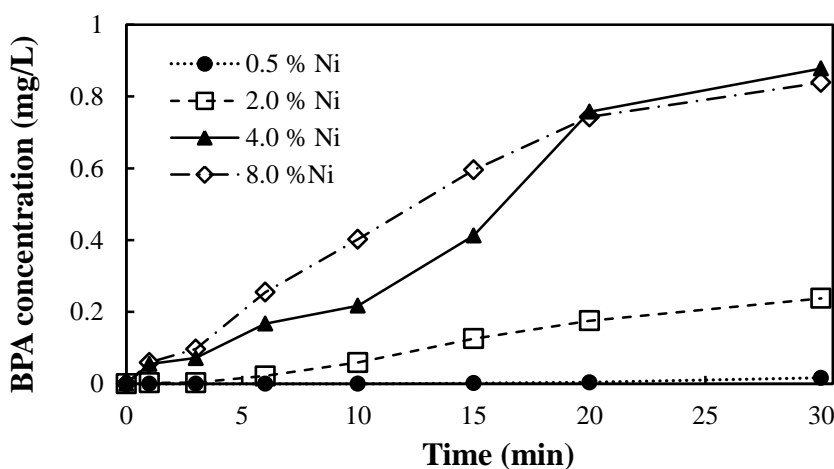

Figure S4 The concentration BPA generated from TBBPA by Ni/Fe nanoparticles with various Ni content ([Ni/Fe]= 2.0 g/L and [TBBPA]=5.0 mg/L).

83

Table S1 The removal rate constants and removal efficiencies of TBBPA by NZVI and Ni/Fe nanoparticles at various percentages of copper.

Ni content (%)	k (min^{-1})	Removal efficiency (%)
0[a]	0.478[a]	99.6[a]
0.5	0.050	78.3
2	0.149	98.2
4	0.208	100[b]
8	0.119	96.4

[a] TBBPA was removed by NZVI in 13 hour.

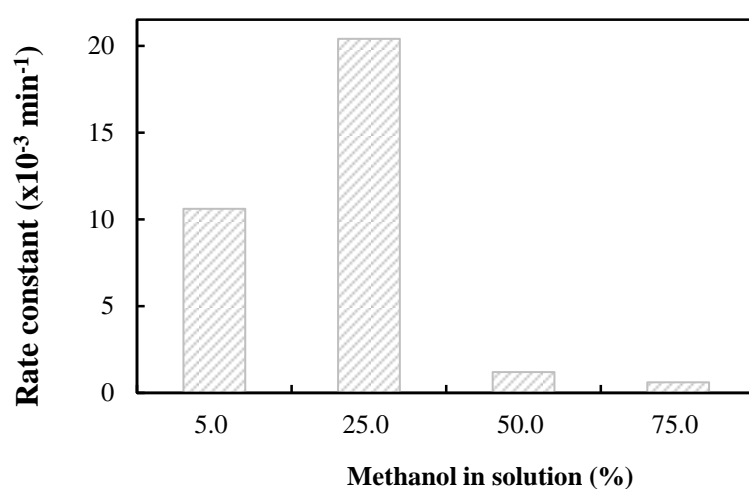[b] The method detection limit of TBBPA is 0.1 mg/L.

Fig. S5. The removal rate constant of TBBPA by Cu/Fe nanoparticles with various methanol cosolvent fraction ([TBBPA]= 5mg/L and [Cu/Fe]= 4g/L).
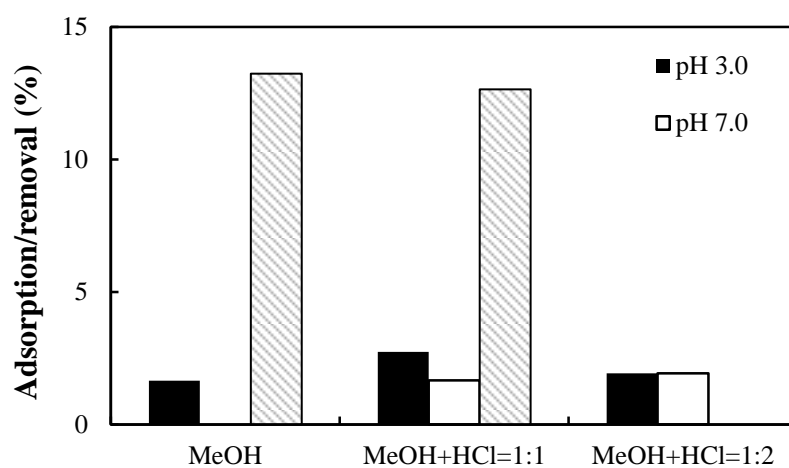

Fig. S6. TBBPA adsorption in total removal with different extraction method with various pH.